ANALYSIS OF COMPOSITE STRUCTURES WITH CURVATURE UNDER TEMPERATURE ENVIRONMENT

by

MUTHU RAM PRABHU ELENCHEZHIAN

Presented to the Faculty of the Graduate School of

The University of Texas at Arlington in Partial Fulfillment

of the Requirements

for the Degree of

MASTER OF SCIENCE IN AEROSPACE ENGINEERING

THE UNIVERSITY OF TEXAS AT ARLINGTON

May 2017

Acknowledgements

I would like to express my sincere thanks to Dr. Wen S Chan, my supervising professor, for his guidance, kindness, patience and motivation towards this thesis work. He has served as my mentor and guided me even before I applied to UTA. I learnt a lot of knowledge and skills from him through the fundamentals of composites and advanced composite courses. I have been surprised several times on his knowledge of composites. I am proud to be his last master's thesis student.

I would express my gratitude to Dr. Kenneth Reifsnider and Dr. Andrey Beyle for their time and effort to serve on my committee.

Next I would like to thank Dr. Kenneth Reifsnider and Dr. Rassel Raihan, my supervisors at UTA Research Institute, who have guided me through my academic and professional path. Without their motivation I could not have done multiple research work. I would also like to thank Dr. Kent Lawrence for offering Advanced Finite Element Methods course and guiding a lot through my thesis work. This thesis would not have been done without his support.

I would like to thank Sidhant Singh, Wei-Tsen Lu, Priyanshu Kumar Banerjee and Vamsee Vadlamudi for guiding me through my work during tough times.

Finally, I would like to express my sincere thanks to my parents who believed in me and supported me to fulfil my dreams, and my beloved friends Nirmal Kumar Umapathy and Sunitha Ravichandran for their kind motivation and support.

May 22, 2017

Abstract

ANALYSIS OF COMPOSITE STRUCTURES WITH CURVATURE

UNDER TEMPERATURE ENVIRONMENT

Muthu Ram Prabhu Elenchezhian, MS Aerospace Engineering

The University of Texas at Arlington, 2017

Supervising Professor: Wen S Chan

Composite structures are frequently exposed to environments with change in temperatures during their service life. The thermal behaviours of the laminated composite structures are more pronounced than that of the structures made of isotropic materials. For the structures under thermal environment, extensive studies have been conducted to investigate the induced thermal stresses and deformation of composite laminated plates by linear/non-linear analysis and composite structures by finite element analysis.

The main focus of this study is concentrated on development of an analytical method for analyzing composite thin shells and/or moderate curved beam structures under temperature environment. This includes the derivation of closed form expression for evaluating deformation/stresses of composite laminates and curved beams using a modified Classical Lamination Plate Theory with curvature, respectively. The present results are validated by 2D and 3D finite element models. Parametric study was done on the thermal stresses of curved beams with varying boundary conditions, ply stacking sequence, radius of beam curvature under various temperatures

Table of Contents

List of Illustrations

List of Tables

Chapter 1

INTRODUCTION

1.1 Introduction to Composite Materials

The Term "Composite" signifies "comprised of two or more different parts." A composite material contains at least two or more elements which are combined together in a macroscopic scale. The material formed has the properties and performance greater than those of the constituent material acting independently. The composite materials have the fibers and matrix as the main phases. As the stiffness and strength are provided by fibers to the composite material, matrix binds them together providing the load transfer strength. Also, the matrix accounts for the shear strength and in-plane transverse strength. The fiber matrix Interphase plays a significant factor in controlling the delamination of the material, failure mechanisms, fracture toughness, stress-strain behavior and failure propagation.

Composite materials have the advantages of being lightweight, possessing excellent corrosion resistance, fatigue resistance and high strength to weight ratio compared to the conventional materials. Advanced Composites are extensively used as a substitute to metallic structures.

Composite structures are used in a variety of applications such as civil constructions, aerospace, automotive, marine, biomedical industries and sports products.

The characteristics of composites such as high specific strength, low density, and high specific stiffness make composites highly advantageous in primary and secondary load carrying structures of military and civil aircrafts. The recognition of composites in civil aviation is by its use in the world largest airliner, Airbus A380 and in Boeing 787. Nearly 50% of the weight of the Boeing 787, including its fuselage and wings are made up of composites.

In 1960's, assuming the stress in each ply of laminate to be planar, a theory was developed to analyze the stress-strain of each laminae. This phenomenon is widely referred as the “Classical Lamination Theory”. However, the different material properties between each layer of laminates produce significant inter-laminar stresses. Even in fragile plate, the inter-laminar stresses are three-dimensional near the edges. Henceforth, as the plane stress condition is assumed in CLT, it is not applicable in the locality of the free edge.

Shell - a thin-walled body, with the middle of the surface being curved in at least one direction. A cylindrical shell, as well as conical shell, has its middle surface curved because it has only one direction. But, in the case of a spherical shell curvature exists in both directions. Such mundane shells as a front fender of a car or an egg shell are an example of double curvature in shells. Shell theory is significantly complicated, compared to beam and plate theory because of this curvature. Then to complicate the shell theory with all of the material complexities associated with laminated composite materials makes shell theory of composite materials very complicated, and a great challenge.

Design and analysis of the composite structure are validated on their performance by the following methodologies – finite element method, analytical solutions, and experimental testing. Although it is a time consuming, expensive and tedious process, composites are typically certified by experimental test methods and not through analysis. In such instances, finite element method takes upper hand as it is compatible with large convoluted structures with high accuracy. It is also necessary to come up an efficient analytical method to analyze the composite structures. Therefore, a simplified method can be used to carry out the initial analysis using the analytical or theoretical results. Also, once the parameters are input into the coding software such as MATLAB, it can be comfortably modified and the new analysis results can be obtained. After validation of analytical solution with finite element model, more complexities can be added to the model and complex analysis can be done. This ensures managing time and saves cost.

1.2 Motivation and Background

The composite structures are frequently exposed to situations with change in temperature throughout their life. The material change behavior of the laminated composites due to thermal effects are more articulated than isotropic materials. In addition, stresses due to thermal loads are induced between and within laminas even when no constraints are applied. Analysis of composites beam structures is often conducted by using finite element method which is time consuming and expensive in design process. Efforts were done by developing analytical method for design validation. Most available analytical methods are complicated to use for a designers and analysts. There is a need for a simple but accurate method for conducting analysis for design variation and optimization studies.

1.3 Literature Review

Hyer and Vogl [1] discussed on the normal, circumferential and axial displacements of elliptical composite cylinders due to a spatially uniform temperature change. They followed the Kantorovich technique and minimization of the total potential energy. They showed that the displacements are characterized by the presence of a circumferential component, lamination sequence and the boundary conditions at ends of the cylinder.

Dano and Hyer [2] presented a method to predict the out of plane displacements components of flat unsymmetrical epoxy matrix composite laminates as they are cooled from their elevated cure temperature. Instead of using the approximation for displacements, their theory directly uses approximations for laminate mid-plane strains. Experimental results were presented to confirm the predictions of the theory.

Hyer [3] in his book Stress Analysis of Fiber-Reinforced Composite Materials, has described the basics of composite materials, Plane stress assumption, Classical Lamination

Theory and various cases of the environmentally induced stresses in the laminates, which served as the basis for the Classical Lamination Theory derivation.

Duan et.al. [4] presented the finite element method model for predicting the large thermal deflection in the composite plates embedded with pre-strained shape memory alloys. For the large thermal deflections, the in-plane strain and the curvature vectors are defined from von Karman strain displacement relation.

Khdeir et.al. [5] researched on the analytical method using the state space approach in conjunction with Levy method for doubly curved cylindrical and spherical shells. Various Boundary conditions were analyzed. The third order theory (HSDT), first order theory (FSDT) and classical theory (CST) were used to obtain the governing equations.

Patel et.al. [6] determined the relationship between the maximum deflection and temperature rise to evaluate the minimum temperature parameter that causes a bifurcation of shell deformation from axisymmetric deformation mode to the asymmetric one in cross-ply laminated composite conical shells by finite deflection analysis. 12 conclusions were made from this research work, which has a significant impact on the conical shells analysis.

Chitikela et.al. [7] developed an analytical method for predicting the critical buckling temperature and natural frequency of symmetric composite box-beam subjected to the temperature gradient. The governing equations were obtained by the small deflection theory and the D Alembert's method. It is inferred that the change in the ply orientation angle cannot overcome the effect of the thermal stress on the natural frequency of a composite box-beam.

Chang et.al. [8] derived the governing equations for nonlinear thermal buckling and post buckling of cross-ply laminated composite beams subjected to temperature rise. The equations were derived based on the Reddys higher order shear deformation plate theory and Von Karman’s geometry nonlinear theory. Their theoretical and numerical results show

that the different thermal expansion coefficient ratio, elastic moduli ratio, and shear stiffness ratio will influence the non-dimension critical buckling temperature.

Xiang and Chen [9] studied on the thermal bending response of laminated composite plates subjected to sinusoidal temperature distribution.

Mackerle [10] developed a bibliography that has the finite elements analysis of the sandwich structures – for isotropic and composite materials from the theoretical as well as practical points of view. He included the special finite elements developed for the analysis of sandwich beams, plates, panels, and shells. He also concentrated on topics like increased temperature, thermal expansion, degradation of elastic properties and viscoelastic effect.

Li and Zhao [11] has derived the exact solutions for the In-Plane displacements of Curved Beams under thermal Load with various end restrictions. Their work included a real multi-span curved bridge subjected to concentrated loads caused by friction force on top of bridge piers and thermal load due to the temperature difference.

Roos, Hormann and Behrens [12] has done immense work on the shell and solid modeling of the composite structures as a base for simulation driven optimization processes.

Aggarwal and Sivaneri [13] has formulated a higher order finite element method for generating the accurate distributions of the stresses and strains in the curved beams. They also proposed a unique curved-beam finite element.

Chan and his students have done a plenty of work on the composite curved beams and composite tubular structures.

Demirhan and Chan [14] derived two analytical models for evaluating the stiffness matrix of the composite tubes by mapping the tubular wall laminates into an equivalent laminate using the laminated plate theory and laminated shell theory. The curvature and stacking sequence effects on axial and bending stiffness were studied.

Wei-Su and Chan [15] derived the closed form solutions for tubular and rectangular cross sections for evaluating the thermal induced stresses.

Nguyen and Chan [16] investigated on the laminate stresses in a curved laminated beam subjected to pure bending moments. A closed form relationship of the laminate constitutive equations was developed. They also developed a FEM Model for the isotropic and orthotropic material and researched on the variation of the tangential and radial stress on changing in curvature, stacking sequence and fiber orientation.

Mahadev and Chan [17] developed a novel mathematical framework to predict the key structural characteristics such as axial stiffness, bending stiffness and centroid for thin walled composite shells. They also incorporated the design and manufacturing of a novel ad-hoc test- fixture setup to experimentally characterize the extension-bending behavior in open cross-section curved composite strips.

1.4 Objective of the Thesis

The primary purpose of the thesis is to obtain the analytical solution for calculating the thermal deformation of the curved beam and to investigate the effect of the deformation of various laminate sequences and different thickness of the curved beam. Also, the effect of the change in thickness of the curved beam along the circumferential direction is investigated for various temperatures.

1.5 Outline of the Thesis

Chapter 1 is introduction of composites, its applications, need for the study and literature review.

Chapter 2 gives a brief review of the classical lamination theory for a plate. It also includes the analytical solution for the deflection of the composite under thermal load. Lastly, finite element 2D modeling of a composite plate, subjected to thermal load is developed and the thermal deformations are obtained.

Chapter 3 describes the curved beam theory, composite shell theory and analytical solution for the deflection of the semi-circular beam and curved beam under thermal loading conditions. It also includes the 3D-solid finite element modeling of the semi-circular beam and curved beam subjected to the thermal load and the deflection of the beams.

Chapter 4 evaluates the results obtained from the analytical and finite element solutions of the plate and the curved beam from Chapters 2 and 3. The deformation change due to the variation of the thickness under the thermal environment is also included.

Chapter 5 comprises of conclusions and future work for the research.

Chapter 2

LAMINATES

This chapter includes the review of the Classical Lamination Theory for a plate. Later the analytical solution for the evaluation of the deformation of the plate under thermal load is discussed. Finally, a 2D shell and 3D solid finite element model are developed to validate the deformation.

2.1 Review of the Classical Lamination Theory

2.1.1 Lamina Constitutive Equation

The composite analysis has two coordinate systems – the x-y-z depicts the global coordinate system, and the 1-2-3 coordinate illustrate the local coordinate system. The fiber direction, transverse fiber direction and direction perpendicular to in-plane ply are indicated by the 1, 2 & 3 in the local coordinates.

For a layer, the stress/strain relationship is given as

$$\begin{bmatrix} \varepsilon_1 \\ \varepsilon_2 \\ \varepsilon_3 \\ \gamma_{13} \\ \gamma_{23} \\ \gamma_{12} \end{bmatrix} = \begin{bmatrix} S_{11} & S_{12} & S_{13} & 0 & 0 & 0 \\ S_{12} & S_{22} & S_{23} & 0 & 0 & 0 \\ S_{13} & S_{23} & S_{33} & 0 & 0 & 0 \\ 0 & 0 & 0 & S_{44} & 0 & 0 \\ 0 & 0 & 0 & 0 & S_{55} & 0 \\ 0 & 0 & 0 & 0 & 0 & S_{66} \end{bmatrix} \begin{bmatrix} \sigma_1 \\ \sigma_2 \\ \sigma_3 \\ \tau_{13} \\ \tau_{23} \\ \tau_{12} \end{bmatrix} \tag{2.1}$$

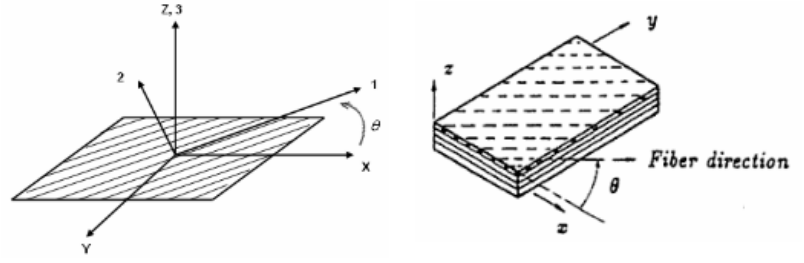

Figure 2.1 Coordinate Systems of the Lamina and Laminate

Since the lamina is thin in composites, plane stress condition is given as

$$\sigma_3 = 0 \qquad \tau_{23} = 0 \qquad \tau_{13} = 0 \tag{2.2}$$

Hence, the relationship between stress and strain for a lamina can be simplified as

$$[\varepsilon]_{1-2} = \begin{bmatrix} \varepsilon_1 \\ \varepsilon_2 \\ \gamma_{12} \end{bmatrix} = \begin{bmatrix} S_{11} & S_{12} & 0 \\ S_{12} & S_{22} & 0 \\ 0 & 0 & S_{66} \end{bmatrix} \begin{bmatrix} \sigma_1 \\ \sigma_2 \\ \tau_{12} \end{bmatrix} \tag{2.3}$$

And

$$\varepsilon_3 = S_{13}\sigma_1 + S_{23}\sigma_2 \neq 0 \tag{2.4}$$

The elements of the compliance matrix [S] are the functions of elastic constant of the composite lamina and are given as

$$S_{11} = \frac{1}{E_1} \qquad S_{12} = -\frac{v_{12}}{E_1}$$

$$S_{22} = \frac{1}{E_2} \qquad S_{13} = -\frac{v_{13}}{E_1} \tag{2.5}$$

$$S_{33} = \frac{1}{E_3} \qquad S_{23} = -\frac{v_{23}}{E_2}$$

$$S_{66} = \frac{1}{G_{12}}$$

The reduced compliance matrix for a thin layer can be inverted to form the reduced stiffness matrix from equation 2.3

$$[\sigma]_{1-2} = \begin{bmatrix} \sigma_1 \\ \sigma_2 \\ \tau_{12} \end{bmatrix} \begin{bmatrix} Q_{11} & Q_{12} & 0 \\ Q_{12} & Q_{22} & 0 \\ 0 & 0 & Q_{66} \end{bmatrix} \begin{bmatrix} \varepsilon_1 \\ \varepsilon_2 \\ \gamma_{12} \end{bmatrix} \tag{2.6}$$

The stiffness matrix [Q] elements are expressed as

$$Q_{11} = \frac{E_1}{1-v_{12}v_{21}}$$

$$Q_{22} = \frac{E_2}{1-v_{12}v_{21}}$$

$$Q_{12} = \frac{v_{21}E_1}{1-v_{12}v_{21}} = \frac{v_{12}E_2}{1-v_{12}v_{21}} \tag{2.7}$$

$$Q_{66} = G_{12}$$

In equation 2.7, E_1 and E_2 represent Young's modulus of the lamina, G_{12} represents the Shear modulus, and v_{12} represents the Poisson's ratio of the lamina.

2.1.2 Stress – Strain Transformation Matrices

In general, the x-y global coordinate system of the lamina does not coincide with the 1-2 local coordinate system. Hence, the transformation matrices are used to transform the stiffness matrix and strains or stresses from the local to the global coordinate system for an angle-ply.

The stiffness matrix for an angle-ply with respect to global system can be obtained by rotating the stiffness matrix of 0° ply as follows

$$[\overline{Q}]_{x-y} = [T_\sigma(-\theta)][Q]_{1-2}[T(\theta)] \tag{2.8}$$

Where $[T_\sigma]$ and $[T_\varepsilon]$ are the transformation matrices for stress and strain, given by

$$[T_\sigma] = \begin{bmatrix} m^2 & n^2 & 2mn \\ n^2 & m^2 & -2mn \\ -mn & mn & m^2 - n^2 \end{bmatrix}$$
$$[T_\varepsilon] = \begin{bmatrix} m^2 & n^2 & 2mn \\ n^2 & m^2 & -mn \\ -2mn & 2mn & m^2 - n^2 \end{bmatrix} \tag{2.7}$$

Where $m = \cos\theta$ and $n = \sin\theta$

2.1.3 Constitutive Equation for the Laminate

The "Lamination Theory", also called as the "Classical Laminated Plate Theory" or as the "Classical Lamination Theory", abbreviated by CLPT or CLT, is the basic procedure to obtain the stiffness matrices for the laminate, mid-plane strains, and curvatures for the laminate, In-plane stresses and strains for each lamina.

Basic Assumptions of the Classical Lamination Theory are

1. Laminate is obtained by bonding several laminae of different fiber orientations
2. Individual lamina of the laminate has its own principal coordinate system
3. A reference coordinate system is introduced common to all the laminas which is set at the mid-plane of the laminate

4. The laminate is thin and wide, i.e., The Plane stress condition is enforced
5. A perfect bond exists between the various laminas
6. The cross-sectional plane of the laminate remains plane after deformation
7. Each lamina and entire laminate behave linearly elastic

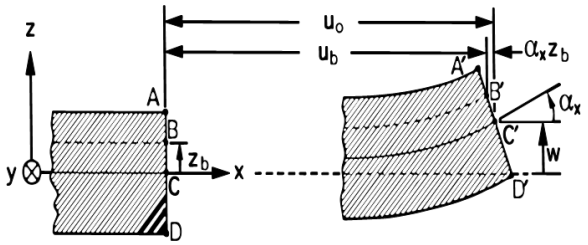

Figure 2.2 Laminate Section under Deformation

The lamina is assumed to bend without slipping over each other, and the cross-section of lamina remains unwrapped. Hence, the displacement of the mid-plane is assumed to be

$$u_o = u_o(x,y)$$
$$v_o = v_o(x,y) \quad (2.10)$$
$$w_o = w_o(x,y)$$

The displacement at any point on the laminate is given by

$$u = u_0 - z\frac{\partial w}{\partial x}$$
$$v = v_0 - z\frac{\partial w}{\partial x} \quad (2.11)$$
$$w = w_0$$

Where u_0 , v_0 and w_0 refer to the displacements in the x, y and z-direction but are the function of x and y only. These displacements are in the reference or mid-plane.

From equation 2.11, The Strain-Displacement relation at any point can be given as

$$\varepsilon_x = \frac{\partial u}{\partial x} = \frac{\partial u_0}{\partial x} - z\frac{\partial^2 w_0}{\partial x^2}$$

$$\varepsilon_y = \frac{\partial v}{\partial x} = \frac{\partial v_0}{\partial x} - z\frac{\partial^2 w_0}{\partial y^2} \quad (2.12)$$

$$\gamma_y = \frac{\partial u}{\partial x} + \frac{\partial v}{\partial x} = \frac{\partial u_0}{\partial x} + \frac{\partial v_0}{\partial x} - 2z\frac{\partial^2 w_0}{\partial x \partial y}$$

For simplicity, we rewrite the equation 2.12 in the matrix form

$$\begin{bmatrix} \varepsilon_x \\ \varepsilon_y \\ \gamma_{xy} \end{bmatrix} = \begin{bmatrix} \varepsilon_x^0 \\ \varepsilon_y^0 \\ \gamma_{xy}^0 \end{bmatrix} + z\begin{bmatrix} \kappa_x \\ \kappa_y \\ \kappa_{xy} \end{bmatrix}$$

Where,

$$\varepsilon_x^0 = \frac{\partial u_0}{\partial x}$$

$$\varepsilon_y^0 = \frac{\partial v_0}{\partial x}$$

$$\gamma_{xy}^0 = \frac{\partial u_0}{\partial x} + \frac{\partial v_0}{\partial x} \quad (2.13)$$

$$\kappa_x = -z\frac{\partial^2 w_0}{\partial x^2}$$

$$\kappa_y = -z\frac{\partial^2 w_0}{\partial y^2}$$

$$\kappa_{xy} = -2z\frac{\partial^2 w_0}{\partial x \partial y}$$

Where 2.13 represents the mid-plane strains and curvatures.

2.1.4 Stress and Strain of Lamina in Laminate Coordinates

The strains in the kth layer is given by

$$\left[\varepsilon_{x-y}\right]_k = [\varepsilon^0] + z_k[\kappa]$$

$$\begin{bmatrix} \varepsilon_x \\ \varepsilon_y \\ \gamma_{xy} \end{bmatrix}_k = \begin{bmatrix} \varepsilon_x^0 \\ \varepsilon_y^0 \\ \gamma_{xy}^0 \end{bmatrix} + z_k\begin{bmatrix} \kappa_x \\ \kappa_y \\ \kappa_{xy} \end{bmatrix} \quad (2.14)$$

The stresses of the k[th] layers in the laminate is given by

$$\left[\sigma_{x-y}\right]_{k^{th}} = [\bar{Q}_{x-y}]_{k^{th}} . [\varepsilon_{x-y}]_{k^{th}} \tag{2.15}$$

$$\left[\sigma_{x-y}\right]_{k^{th}} = \left[\bar{Q}_{x-y}\right]_{k^{th}} ([\varepsilon^{0}{}_{x-y}] + z_{k^{th}}\left[\kappa_{x-y}\right])$$

2.1.5 Force and Moment Resultants of Laminate

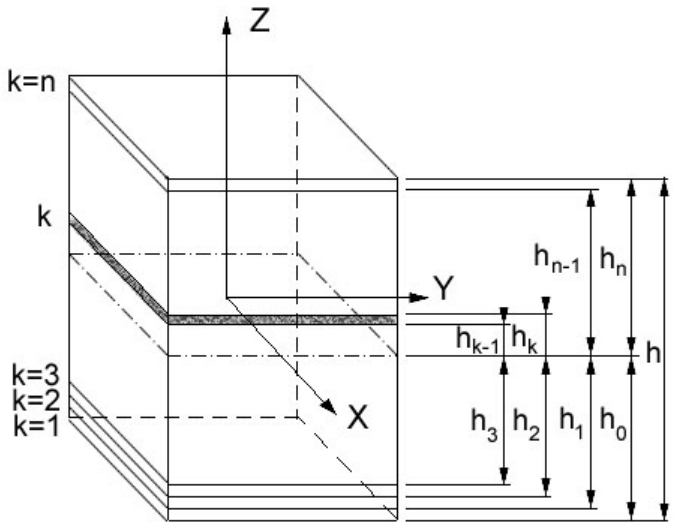

Figure 2.3 Composite Laminate with n-Layers

The general relationship for the Force/Moments and Strain of the laminate is given by

$$\begin{bmatrix}\bar{N}\\ \bar{M}\end{bmatrix} = \begin{bmatrix}A & B\\ B & D\end{bmatrix}\begin{bmatrix}\varepsilon^{0}\\ \kappa\end{bmatrix} \tag{2.16}$$

Where $[\varepsilon^{\circ}]$ and $[\kappa]$ represent the mid-plane strain and mid-plane curvatures respectively, given by equation 2.13

The $[\bar{N}]$ and $[\bar{M}]$ are the Force and Moment matrices, are given by

$$\begin{bmatrix}\bar{N}\\ \bar{M}\end{bmatrix} = \begin{bmatrix}N\\ M\end{bmatrix}\begin{bmatrix}N^{T}\\ M^{T}\end{bmatrix} \tag{2.17}$$

Where [N] and [M] represent the applied load and applied moment due to mechanical forces respectively. They are given by the equation

$$[N] = \sum_{k=1}^{n} \int_{4-1}^{4} [\sigma]_k . dz$$

$$[M] = \sum_{k=1}^{n} \int_{4-1}^{4} [\sigma]_k . z . dz \tag{2.18}$$

The force and moment induced due to thermal loads are given by [N^T] and [M^T] as

$$[N^T] = \left\{ \sum_{k=1}^{n} [\bar{Q}]_k . [\alpha_{x-y}]_k . (h_k - h_{k-1}) \right\} . \Delta T$$

$$[M^T] = \frac{1}{2} \left\{ \sum_{k=1}^{n} [\bar{Q}]_k . [\alpha_{x-y}]_k . ({h^2}_k - {h^2}_{k-1}) \right\} . \Delta T \tag{2.19}$$

In equation 2.19, $\left[\alpha_{x-y}\right]_k$ represents the coefficient of thermal expansion (CTE), of k^{th} ply transforming from laminae local to the global coordinate system. ΔT is the difference between applied temperature and room temperature. h^k represents the distance to the top of k^{th} ply as shown in Figure 2.3.

[A], [B], and [D] matrices given in equation 2.16 represents in-plane extensional stiffness matrix, extensional-bending coupling stiffness matrix, and bending stiffness matrix respectively. These are evaluated per unit width of the laminate and are given by

$$[A] = \sum_{k=1}^{n} [\bar{Q}]_k . (h_k - h_{k-1})$$

$$[B] = \frac{1}{2} \sum_{k=1}^{n} [\bar{Q}]_k . ({h^2}_k - {h^2}_{k-1}) \tag{2.20}$$

$$[D] = \frac{1}{3} \sum_{k=1}^{n} [\bar{Q}]_k . ({h^3}_k - {h^3}_{k-1})$$

Where $[\bar{Q}]_k$ is obtained from the transformed reduced stiffness matrix from equation 2.8.

From Equation 2.16,

$$\begin{bmatrix} \varepsilon^{\circ} \\ \kappa \end{bmatrix} = \begin{bmatrix} a & b \\ b^T & d \end{bmatrix} \begin{bmatrix} N \\ M \end{bmatrix} \tag{2.21}$$

Where

$$\begin{bmatrix} a & b \\ b^T & d \end{bmatrix} = \begin{bmatrix} A & B \\ B & D \end{bmatrix}^{-1} \tag{2.22}$$

Equation 2.21 gives the strain and curvature at the mid-plane of the laminate.

2.1.6 Thermal Strains

Composites have their tendency to change their characteristics when exposed to temperature. These changes in their characteristics are due to their Coefficient of Thermal Expansion (CTE). In general observation, the characteristics of the change of structural response due to temperature are identical to the change of moisture. Hence, by changing the temperature terms to moisture, or by adding the same temperature terms with moisture coefficients, the composite laminate can be analyzed for hygro-thermal environments.

The Thermal Strain of the laminate is given by

$$\varepsilon_i^T = \alpha_i \Delta T \tag{2.23}$$

Where α_i represents the CTE and i =1,2 and 3 represents the normal components of the thermal strain and ΔT represents the difference in temperature.

2.2 Analytical Method for Deformation in Laminate

As Discussed before, we obtain the [A], [B] and [D] Matrices from the Classical Lamination Theory.

The relationship between load and deformation of laminate can be written in terms of the strain and curvature of mid-plane as

$$\begin{bmatrix} \bar{N} \\ \bar{M} \end{bmatrix} = \begin{bmatrix} A & B \\ B & D \end{bmatrix} \begin{bmatrix} \varepsilon^{\circ} \\ \kappa \end{bmatrix} \tag{2.24}$$

$[\bar{N}]$= [N] + $[N]^T$, where $[\bar{N}]$ represents the total force applied, [N] is the mechanical force and $[N]^T$ is the Thermal Force applied.

Similarly, $[\bar{M}]$ = [M] + $[M]^T$, where $[\bar{M}]$ represents the total bending moments applied per unit width, [M] is due to mechanical load and $[M]^T$ is due to the thermal load.

From equation (2.24)

$$\begin{bmatrix} \varepsilon^{\circ} \\ \kappa \end{bmatrix} = \begin{bmatrix} a & b \\ b^T & d \end{bmatrix} \begin{bmatrix} \bar{N} \\ \bar{M} \end{bmatrix} \tag{2.25}$$

As there is no mechanical load applied, and only Thermal load is applied

$$[N]^M = [M]^M = 0 \tag{2.26}$$

Hence equation (2.25) becomes

$$\begin{bmatrix} \varepsilon^{\circ} \\ \kappa \end{bmatrix} = \begin{bmatrix} a & b \\ b^T & d \end{bmatrix} \begin{bmatrix} N^T \\ M^T \end{bmatrix} \tag{2.27}$$

2.2.1 Plate A – Symmetrical Balanced Laminate

For a symmetrical balanced laminate only under the thermal Load,

$[B] = 0$; $[M]^T = 0$; $[N_x]^T \neq 0$; $[N_y]^T \neq 0$; $[N_{xy}]^T = 0$;

Substituting these conditions in (2.27), We get the mid-plane strains to be,

$$\varepsilon^{\circ}_x = a_{11}N_x^T + a_{12}N_y^T = \frac{\partial u_o}{\partial x} \tag{2.28}$$

$$\varepsilon^{\circ}_y = a_{12}N_x^T + a_{22}N_y^T = \frac{\partial v_o}{\partial y} \tag{2.29}$$

$$\gamma^{\circ}_{xy} = 0 \tag{2.30}$$

Integrating Equations (2.28), (2.29) and (2.30) and solving using the boundary conditions, we get

$$U_o = (a_{11}N_x^T + a_{12}N_y^T) x \quad (2.31)$$

$$V_o = (a_{12}N_x^T + a_{22}N_y^T) y \quad (2.32)$$

Equations (2.31) and (2.32) gives the X and Y deformation for a symmetrical balanced laminate under the thermal Load.

2.2.2 Plate B – Symmetrical Un-Balanced Laminate

For a symmetrical un-balanced laminate only under the thermal load,

$$[B] = 0 ; \quad [M]^T = 0 ; \quad [N_x]^T \neq 0 ; \quad [N_y]^T \neq 0 ; \quad [N_{xy}]^T \neq 0 ;$$

Substituting these conditions in (2.27), we get the mid-plane strains to be,

$$\varepsilon^\circ_x = a_{11}N_x^T + a_{12}N_y^T + a_{16}N_{xy}^T \quad (2.33)$$

$$\varepsilon^\circ_y = a_{12}N_x^T + a_{22}N_y^T + a_{26}N_{xy}^T \quad (2.34)$$

$$\gamma^\circ_{xy} = a_{16}N_x^T + a_{26}N_y^T + a_{66}N_{xy}^T \quad (2.35)$$

Integrating equations (2.33), (2.34) and (2.35) and solving using the boundary conditions, we get

$$U_o = \varepsilon^\circ_x x + 0.5\, \gamma^\circ_{xy} y \quad (2.36)$$

$$V_o = \varepsilon^\circ_y y + 0.5\, \gamma^\circ_{xy} x \quad (2.37)$$

The Equations (2.36) and (2.37) gives the X and Y deformation for a Symmetrical Un-Balanced Laminate under the Thermal Load.

2.2.3 Plate C & D – Unsymmetrical Laminates

For an un-symmetrical laminate only under the thermal load,

$$[M]^T \neq 0 ; \quad [N_x]^T \neq 0 ; \quad [N_y]^T \neq 0 ; \quad [N_{xy}]^T \neq 0 ;$$

Hence (2.27) becomes

$$\begin{bmatrix} \varepsilon^{\circ} \\ \kappa \end{bmatrix} = \begin{bmatrix} a * N^T + & b * M^T \\ b^T * N^T + & d * M^T \end{bmatrix} \tag{2.38}$$

Integrating Equations in (2.28) and solving using the boundary conditions, we get

$$U_o = \varepsilon^{\circ}_x \, x + 0.5 \, \gamma^{\circ}_{xy} \, y \tag{2.39}$$

$$V_o = \varepsilon^{\circ}_y \, y + 0.5 \, \gamma^{\circ}_{xy} \, x \tag{2.40}$$

$$W_o = -\left(0.5 \, \kappa_x \, x^2 + 0.5 \, \kappa_y \, y^2 + 0.5 \, \kappa_{xy} \, x \, y \right) \tag{2.41}$$

Equations (2.39), (2.40) and (2.41) gives the X, Y and Z deformation for an un-symmetrical laminate under the thermal load.

2.2.4 Thickness Change of Laminate under Thermal Load

For a given k^{th} layer of the laminate, the strain in the thickness direction can be written as

$$\varepsilon_{3,k} = S_{13,k}\sigma_{1,k} + S_{23,k}\sigma_{2,k} + \alpha_{3,k}\Delta T \tag{2.42}$$

Where $S_{13,k}$ and $S_{23,k}$ are given in equation (2.5). $\sigma_{1,k}$ and $\sigma_{2,k}$ can be obtained from the in-plane analysis of the laminate under N^T and/or M^T.

The thickness change of the k^{th} layer is

$$\Delta t_k = \varepsilon_{3,k} t_k \tag{2.43}$$

t_k is the thickness of the k^{th} layer. The total thickness change Δt_{total} can be

$$\Delta t_{total} = \sum_{k=1}^{n} \Delta t_k \tag{2.44}$$

and the average strain in the thickness direction can be written as

$$\varepsilon_3 = \frac{\Delta t_{total}}{\sum_{k=1}^{n} t_k} \tag{2.45}$$

2.3 Finite Element Modelling

This Chapter describes the geometry of the structures, materials used in the model, construction and meshing of the model and the boundary conditions used in every structure. ANSYS Mechanical APDL 17.0 and 17.2 were used to develop the 2-D and 3-D Finite Element Model. 2-D model is a smeared model and 3-D model is a solid layer by layer model.

2.3.1 Material Used

2.3.1.1 Material Selection

The material used is IM7/8552 – Graphite Fiber-Epoxy Prepreg Manufactured by the Hexcel. Hexcel's HexTow IM7/8552 is the preferred carbon fiber for the most advanced aerospace and industrial applications including Airbus A350 XWB, Eurofighter Typhoon, Boeing 787 and GEnx Engines. It is used in the primary and secondary aircraft applications, space and defense operations in the missiles and space launchers. The cured ply thickness is 0.0072 inch.

2.3.1.2 Material Properties

The material properties used throughout the analysis for all laminates and structures are given in Table 2.1 Below. These properties are obtained for 0° ply laminae at the 72°F room temperature.

The fiber direction, transverse direction and the out of plane direction is indicated by the subscripts 1, 2 and 3 respectively. The young's moduli of the composite ply lamina are represented by constants E_1, E_2 and E_3. The constants v_{12}, v_{13} and v_{23} represent the Poisson's ratio. The constants G_{12}, G_{13} and G_{23} indicate the shear moduli with respect to 1-2, 1-3 and 2-3 planes respectively. The constants α_1, α_2 and α_3 are the coefficients of the thermal expansion of the ply.

Table 2.1 Lamina Properties for IM7/8552

Lamina Properties for IM7/8552 Gr/Ep at 72°F	
E_1	23.35 Msi
E_2	1.65 Msi
E_3	1.65 Msi
v_{12}	0.32
v_{13}	0.32
v_{31}	0.436
G_{12}	0.75 Msi
G_{13}	0.75 Msi
G_{23}	0.58 Msi
t_{ply}	0.0072 inch
α_1	-5.5×10^{-8} / °F
α_2	17.22×10^{-6} / °F
α_3	17.22 10^{-6} / °F

2.3.2 Laminate Sequence

There are four different stacking sequences which are being considered for the analysis of the structures. Each laminate is made up of 8 plies. They are listed below in Table 2.2

Table 2.2 Laminate Stacking Sequence

Model Name	Type	Sequence
A	Symmetric Balanced	$[45 / -45 / 0]_S$
B	Symmetric Un-Balanced	$[45_2 / 0]_S$
C	Un-Symmetric Balanced	$[45 / -45 / 0]_{2T}$
D	Un-Symmetric Un-Balanced	$[45_2 / 0]_{2T}$

2.3.3 Element Type

The element types that are used for modeling of composite materials in ANSYS are SHELL181, SHELL281, SOLSH190, SOLID185 Structural / Layered Solid, and SOLID186 Structural / Layered Solid. Based on our need, application and type of results desired, the corresponding element can be chosen. These data regarding the elements are obtained from ANSYS documentation. – ANSYS APDL Element Reference Manual [22].

"*SHELL181 and SHELL 281*

SHELL 181 is a 4-node 3-D shell element with 6 degrees of freedom at each node, whereas SHELL 281 is an 8-node element. SHELL 181 element has capabilities of full nonlinear including large strain and allows 255 layers. SHELL 281 can analyze thin to moderately thick structures. It is also used for linear, large rotation and/or large stain nonlinear applications

SOLSH190 -- 3-D Layered Structural Solid Shell

An 8-node 3-D solid shell component with three degrees of freedom for each node. The element can be utilized for simulating shell structures with an extensive variety of thickness (from thin to modestly thick). It has full nonlinear capabilities including analysis of large strains. The element can be stacked to demonstrate through-the-thickness discontinuities.

SOLID185 Layered Solid

3-D 8-Node Layered Solid utilized for 3-D modeling of solid structures. It is characterized by eight nodes with 3 DOF at each node. It has plasticity, hyper-elasticity, stress stiffening, creep, large deflection, and large strain capabilities. It also has mixed formulation capability for simulating deformations of nearly incompressible elasto-plastic materials, and fully incompressible hyper elastic materials. The component is also considered for prism and tetrahedral degenerations when used in irregular regions. Different element technologies such as B-bar, uniformly reduced integration, and enhanced strains are supported. SOLID278 is a companion thermal element.

SOLID186 Layered / Structural Solid

A higher-order version of the SOLID185 element. SOLID279 is a companion thermal element.

In this research work, we choose SHELL 281 for the 2D plate modelling and SOLID186 for the 3D modelling. Each of these elements is discussed here in detail. SHELL 281 is modelled as a shell section with smeared properties, whereas the SOLID186 is used to model solid layers of orthotropic plies, layer by layer.

SHELL281

SHELL281 is suiTable for analyzing thin to moderately-thick shell structures. It is an 8 noded element with 6 degrees of freedom at each node: translations in the x, y, z - axes, and rotations about the x, y, z-axes. (When using the membrane option, the element has translational degrees of freedom only). SHELL281 is good for linear, large rotation, and/or large strain nonlinear applications. Change in shell thickness is accounted for in nonlinear analyses. SHELL281 may be used for layered applications for modeling composite shells or sandwich construction. The accuracy in modeling composite shells is governed by the first-order shear-deformation theory (usually referred to as Mindlin-Reissner shell theory). The element formulation is based on logarithmic strain and true stress measures. The element kinematics allow for finite membrane strains (stretching). However, the curvature changes within a time increment are assumed to be small.

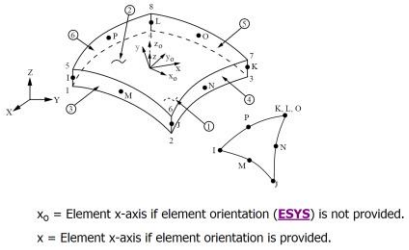

Figure 2.4 SHELL281 Geometry

SHELL281 Assumptions and Restrictions

- *Zero thickness elements or elements tapering down to a zero thickness at any corner are not allowed (but zero thickness layers are allowed).*
- *If multiple load steps are used, the number of layers may not change between load steps.*
- *When the element is associated with pre-integrated shell sections, additional restrictions apply.*
- *No slippage is assumed between the element layers. Shear deflections are included in the element; however, normal to the center plane before deformation are considered to remain straight after deformation.*
- *The transverse shear stiffness of the shell section is estimated by an energy equivalence procedure. The accuracy of this calculation may be adversely affected if the ratio of material stiffness's (Young's moduli) between adjacent layers is very high.*
- *The calculation of interlaminar shear stresses is based on simplifying assumptions of unidirectional, uncoupled bending in each direction. If accurate edge interlaminar shear stresses are required, shell-to-solid sub modeling should be used.*
- *The section definition permits use of hyperplastic material models and elastoplastic material models in a laminate definition. However, the accuracy of the solution is primarily governed by fundamental assumptions of shell theory. The applicability of shell theory in such cases is best understood by using a comparable solid model.*
- *The through-thickness stress, SZ, is always zero.*
- *The thickness of the shell is assumed to remain constant even in a large-strain analysis.*

Due to these assumptions and constrains we need to have a 3D model to analyze the Strain in the third direction, i.e., the Thickness direction.

SOLID186

SOLID186 is a higher-order 3-D 20-node solid element that exhibits quadratic displacement behavior. It supports plasticity, hyper-elasticity, creep, stress stiffening, large deflection, and large strain capabilities. It also has mixed formulation capability for simulating deformations of nearly incompressible elasto-plastic materials, and fully incompressible hyper-elastic materials. SOLID186 is available in two forms: homogeneous structural solid and layered structural solid.

In SOLID186, we use the homogeneous structural solid to form orthotropic layers. using the layered structural solid will produce a smeared model with smeared results. hence, the homogeneous structural solid will produce more accurate results on deformation of each lamina." [22]

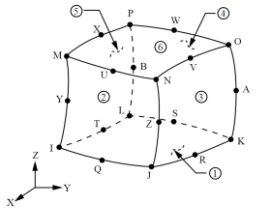

Figure 2.5 SOLID186 Geometry

2.3.4 Development of 2D - Finite Element Model

For 2D modelling, a thin plate was to be modelled. The element type was chosen as SHELL 281. As it was a composite layup, the storage of layer data K8 value was set to All Layers in the options.

Layup of Laminate

Select Sections – Shell – layup – add/edit to create the stacking sequence. The thickness value for each ply and the Angle of fiber orientation of each ply was inputted for all the eight layers. The Plot Section command will display the following Figure 2.6

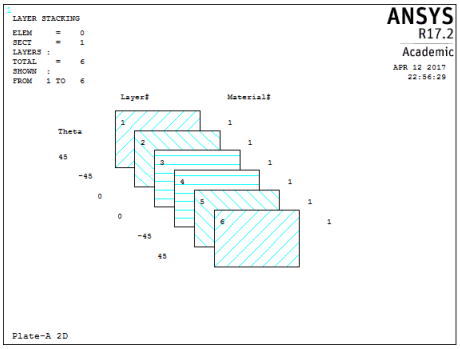

Figure 2.6 Layer Stacking Sequence for Model A

Modelling of the Plate

A Rectangular plate of 2 inches x 1.5 inches was modelled by using the create - area command, keeping the center point as origin (0,0) on the x-y plane as shown in Figure 2.7. The Direction in which the area is created should be taken care. The normal direction should be upwards as per the right-hand rule. If it's vice versa, the results will vary.

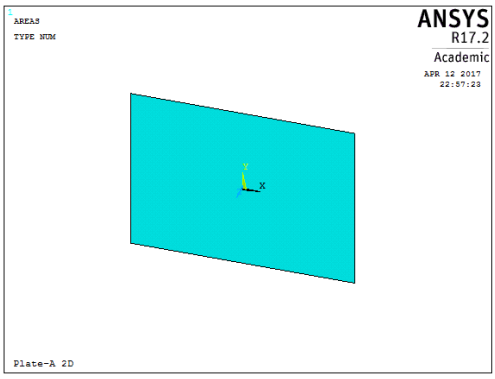

Figure 2.7 2-D Model of the Plate

Meshing

The Meshing was performed by defining the line element size as required along the breadth and width of the plate. Line Element size was set in such a way that the ratio of the thickness of element to any other dimension of the element is not 1:10.

Boundary and Loading Conditions

Displacement

ANSYS requires the structure to be fixed. Hence, the center (0,0) was constrained in all degrees of freedom, so that there will be no transitional motion and no rotational motion at origin on x, y and z direction. (Ux = Uy = Uz = 0 ; Rx = Ry = Rz = 0)

Temperature

A uniform temperature load of 172 °F was applied, such that difference between load temperature and room temperature was 100°F. the model was solved.

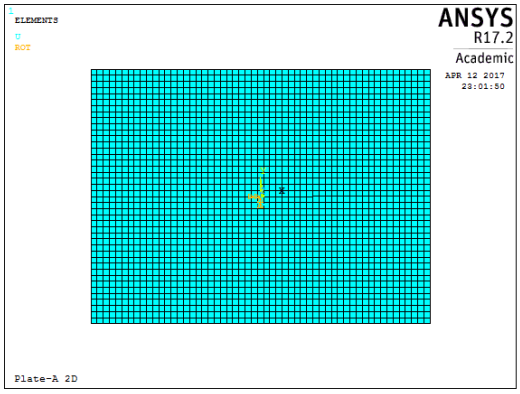

Figure 2.8 Meshed Plate with Load

For thickness option, the element view can be selected in options and plate can be viewed along thickness.

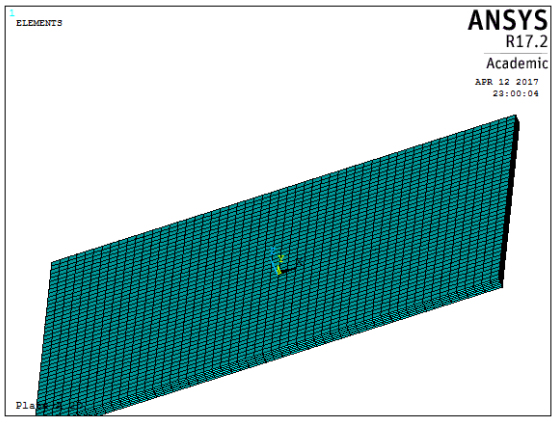

Figure2.9 2-D plate with Thickness

Post Processing

The X, Y and Z component of deformation are obtained for each model. As it is a plate, the 4 nodal points which are the four corners of the rectangle are taken into consideration for comparison with the theoretical values. Plate A and B, which are symmetrical does not have the Z component of deformation, and the Plates C and D has the Z component of deformation due to curvature.

2.3.5 Development of 3D- Finite Element Model

To study the thickness variation of the plates due to thermal load, and include the third dimensional properties in the calculations, a 3D solid model is being created. This will produce more accurate results than the 2D model, as in the 2D analytical and FEM Models, the strain in z-direction is being ignored.

Element type

The SOLID186 – structural solid element is utilized for the 3D modelling of the plate. Each solid layer is been created layer by layer.

Modelling of the Plate

A rectangular volume of 2 inches x 1.5 inches x 0.0072 inch is being created by creating the key points and the volume command. The same command is repeated for five times, to totally create a 6-layer laminate. A single ply and the laminate volume are shown in Figure 2.11.

Orientation of the Plate

Since the plate is made up of 6-layers of solid elements, the orientation of each layer is defined by creating local coordinate systems. While meshing, the local coordinate systems are assigned to each layer.

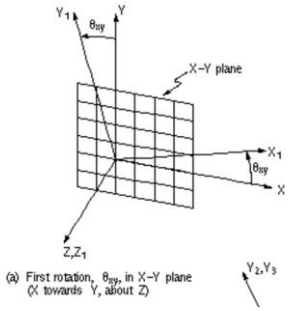

Figure 2.10 Orientation of Each Layer by Local Coordinate System

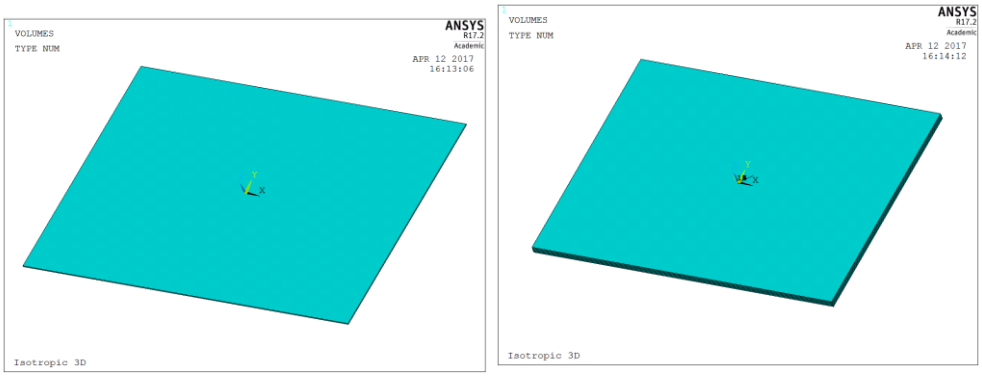

Figure 2.11 Single Ply Laminae and 6-ply Laminate

Meshing

Each ply is meshed individually with respects to its material orientation. Each line of the volume is being selected and the line element size is being defined. Since it is a composite laminate,

the line element size for Z- Direction line is always 1, as the composite plies are not split into elements in the thickness direction. Once the volume attributes and the line element attributes are defined, the volume is meshed. The same procedure is repeated for all the plies. The meshing for a laminae and the laminate is shown in Figure 2.12.

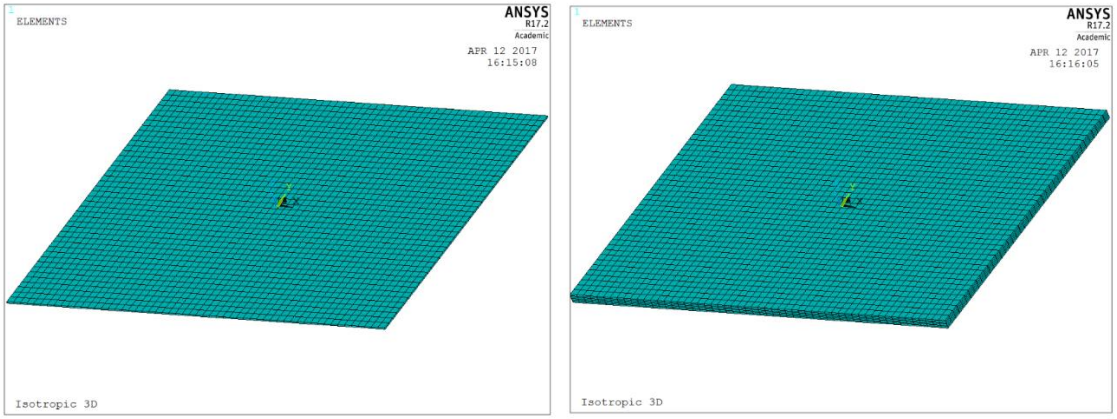

Figure 2.12 Mesh of Each Individual Laminae and Total Laminate

Boundary and Loading Conditions

For the case of 2D plate element, the model was fixed at the center of reference. But for the 3-D solid elements, fixing it only at the center of the plate makes it less constrained. Hence the model was fixed in center of origin in all directions (UX = 0 ; UY = 0 ; UZ = 0) and also the nodes through the thickness direction of the center element (x = 0 ; y = 0 ; z varies) was constrained in the X and Y directions (UX = 0 ; UY = 0) .

Also, the temperature load of 172 °F was being applied with the room temperature set to 72 °F, hence a temperature difference of 100°F is obtained. The model is solved.

The boundary conditions are shown in Figures 2.15(a) and 2.15(b) respectively.

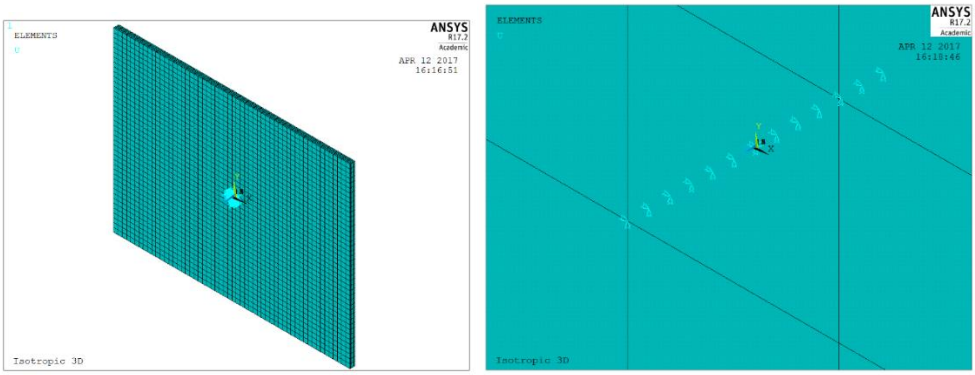

Figure 2.13 Boundary Conditions for a 3-D Model

2.3.5.1 Mesh Convergence

The finite element method is the concept of sub-dividing a body into small discrete elements, which are called as the finite elements. Each finite element has its nodes and interpolation functions. Governing equations are developed for each element, the elements are combined together, and the global governing equation and matrix is obtained. The displacement solutions are obtained by applying the boundary conditions and loads. The general issue that always arises is on the requirement of how small is it need to make the elements so that we can trust the solution. An exact firm answer is not yet available to this issue. Hence, mesh convergence test is necessary. In this mesh convergence test, the model is first meshed with particular size and results are obtained. The mesh is refined to a smaller size than previous and results are obtained. Both the results are compared. If the results have less error percentage, then the first mesh is accepted to be good enough for that particular geometry, loading and boundary conditions. If the results have large error percentage, it will be necessary to try a finer mesh. Finer the mesh is, more is cost, calculation time and memory requirements (both disk and RAM). It is necessary to find the minimum number of elements that delivers a converged solution.

The Convergence requirements can be classified into three groups:

- Completeness: - The elements must possess strong approximation power that captures the analytical solution within the limits of mesh refinement.
- Compatibility: - The displacement continuity between elements should be provided by the shape functions. This is to insure that no material gaps appear as the elements deform. Such gaps would multiply and might absorb or release spurious energy as the mesh refinement continues.
- Stability: - The finite element system must satisfy certain conditions that preclude nonphysical zero-energy modes in elements and the absence of excessive element distortion.

Consistency of FEM is defined by completeness and compatibility between the discrete and mathematical models. A Consistent finite element model is that which passes both completeness and continuity requirements. This is the FEM analog of the famous Lax-Wendroff theorem, which says that consistency and stability imply convergence. Convergent solutions are obtained only using right approach methods as discussed below:

- Proper element type must be chosen.
- Use a fine mesh
- Thin long elements should be avoided
- Stress accuracy must be verified
- Rigid body motion must be prevented
- Reaction forces must be verified
- Inter-element connectivity must be checked

In general practice, the ratio to the thickness to any other side must not be greater than 10. For the mesh convergence study of laminates, 5 models of meshes are been developed and the values of displacements and stress obtained at the node 2, (x = 1, y = -0.75, z=-0.002216) was obtained. For each model, the number of elements were increased.

Table 2.3 Mesh Convergence of Laminates

Model	Ratio of L : B : H	No of Nodes	No of Elements	Displacement at Node 2 (Usum)	Error %
A	20 : 20 : 1	4273	840	1.7428E-3	-
B	16 : 12 :1	9481	1944	1.7363E-3	0.373
C	8 : 6 :1	32585	6936	1.7491E-3	0.737
D	4 : 3 :1	135113	29400	1.7500E-3	0.051
E	2 : 1 :1	781941	172224	1.7500E-3	0.000

2.3.5.2 Validation of the 3-D Finite Element Model

The 3-D finite element model was first validated by using the isotropic material properties. Aluminum AL6061-T6 was chosen as the isotropic material and its properties were used. The properties of the aluminum are

$$E = 10 \text{ Msi} ; v = 0.33 ; \alpha = 14 \times 10^{-6} ; G = 3.75 \text{ Msi}$$

The Deformations in X, Y, Z directions were obtained from the Finite Element Model and compared with the Analytical Solutions.

Deformation of an Isotropic Plate – Analytical Solution

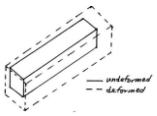

Figure 2.14 Deformation of Isotropic material

When a material undergoes heating or cooling, it undergoes deformation and hence there is a change in length of the material by an amount proportional to the original length and the change in temperature. This change in length is termed as linear thermal expansion, which is given by

$$dl = L_0 \alpha (t_1 - t_0) \qquad (2.46)$$

where

dl = change in length of material (inches)

L_0 = material's initial length (inches)

α = linear expansion coefficient (in/in^{o}F)

t_0 = initial temperature on material (^{o}F)

t_1 = final temperature on material (^{o}F)

Deformation of an Isotropic Plate – 3D Finite Element Model

The X, Y and Z components of deformation of the 3D plate is shown in Figures 2.17 a, b and c respectively..

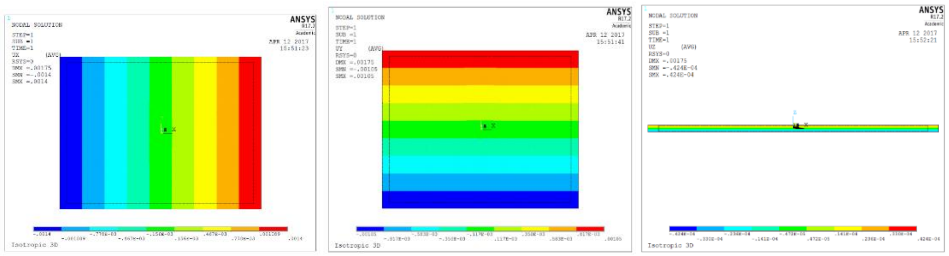

Figure 2.15 Deformation of X, Y, Z direction

Results

The analytical and finite element results are compared in the following Table.

Table 2.4 Comparison of the Analytical and FEM Deformations of the Isotropic Laminate

	Initial Length (inches)	Change in Length (dl) Analytical	Change in Length FEM	Error %
X (Breadth)	2	2.8E-3	2.799E-3	0.035 %
Y (Height)	1.5	2.1E-3	2.0998E-3	0.0095 %
Z (Thickness)	0.0432	0.0604E-3	0.0604E-3	0 %

Since the error percentages are very negligible, the finite element results agree with the theoretical results. Hence, this 3-D model can be used for the composite plates.

Chapter 3

CURVED BEAMS

This chapter begins with the theory on the curved beams, deriving the analytical solution for stresses and deformation of the curved beam laminates. Later the Finite Element Model of the 2D curved plate and 3D curved beam are being developed.

3.1 Geometry of the Curved Beam

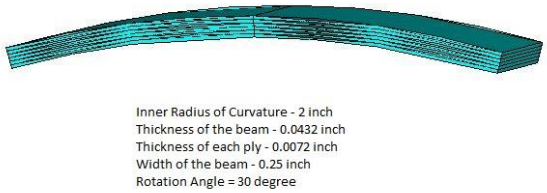

Figure 3.1 Model of Curved Beam

The curved beam section of radius 2 inch and angle of rotation 30 degrees was considered for the analysis. The thickness of each ply was 0.0072 inches, and hence the total thickness of the beam was 0.0432 inches. The mean radius R_m was 2.0216 inches. The length of the curved beam was different for each ply, and it depends on the radius of that ply. The radius of each ply and its corresponding length are given in the Table 3.1

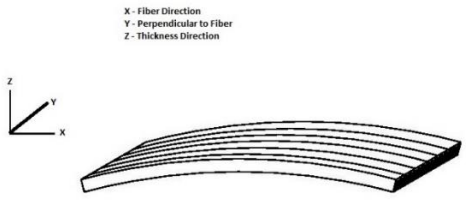

Figure 3.2 Coordinate System of Curved Beam

Ply	Radius (inches)	Length (inches)
1	2	1.0472
2	2.0072	1.0509
3	2.0144	1.0547
4	2.0216	1.0586
5	2.0288	1.0622
6	2.036	1.0660
	2.0432	1.0698

Table 3.1 Radius and Length of Each Ply

As shown in Figure 3.2, the curvature of the beam is along the fiber direction – x direction. Hence each ply has bending along the fiber direction.

3.2 Analytical Solution for Curved Beam

3.2.1 Classical Lamination Plate Theory for Curved Beams

In the previous chapter, we discussed the classical lamination theory for plates. In this Section, the Classical Lamination Plate theory was being used in thin curved beams to derive the strains and curvatures of the laminate. The deformations are obtained from the strains and curvatures by the kinematics equations.

According to the kinematics equations from the bending theory of cylindrical shells [25],

$$\varepsilon_\theta = \frac{1}{R}\frac{\partial u_0}{\partial \theta} - \frac{z}{R(R+z)}\frac{\partial^2 w}{\partial \theta^2} + \frac{w}{R+z}$$

$$\varepsilon_y = \frac{\partial v_0}{\partial y} - z\frac{\partial^2 w}{\partial y^2} \tag{3.1}$$

$$\gamma_{y\theta} = \frac{1}{R+z}\frac{\partial v_0}{\partial \theta} + \frac{R+z}{R}\frac{\partial u_0}{\partial y} - \left(\frac{z}{R} + \frac{z}{R+z}\right)\frac{\partial^2 w}{\partial y \partial \theta}$$

A curved beam is regarded as thin when the ratio h/R is less than 0.1 and higher order terms in the binomial expansion of the term, i.e., $\left(1+\frac{z}{R}\right)^{-1}$ can be neglected.

On further Simplifying equation 3.1 and neglecting z^2 terms, we get

$$\varepsilon_\theta = \frac{1}{R}\frac{\partial u_0}{\partial \theta} - \frac{z}{R^2}\frac{\partial^2 w}{\partial \theta^2} + \frac{w\left(1-\frac{z}{R}\right)}{R}$$

$$\varepsilon_y = \frac{\partial v_0}{\partial y} - z\frac{\partial^2 w}{\partial y^2} \tag{3.2}$$

$$\gamma_{y\theta} = \frac{\left(1-\frac{z}{R}\right)}{R}\frac{\partial v_0}{\partial \theta} + \left(1+\frac{z}{R}\right)\frac{\partial u_0}{\partial y} - \frac{2z}{R}\frac{\partial^2 w}{\partial y \partial \theta}$$

where $\varepsilon_\theta, \varepsilon_y \; and \; \gamma_{y\theta}$ represents the tangential strain, lateral strain, and shear strain respectively and u,v and w represent the displacements in the shell direction respectively.

The strain components are expressed as the sum of the mid-plane strains and mid-plane curvature as

$$\begin{Bmatrix} \varepsilon_\theta \\ \varepsilon_y \\ \gamma_{\theta y} \end{Bmatrix} = \begin{Bmatrix} \varepsilon_\theta^0 \\ \varepsilon_y^0 \\ \gamma_{\theta y}^0 \end{Bmatrix} + z\begin{Bmatrix} \kappa_\theta \\ \kappa_y \\ \kappa_{\theta y} \end{Bmatrix} \tag{3.3}$$

The mid-plane strains and curvatures are given from 3.3 by

$$\varepsilon_\theta^0 = \frac{1}{R}\frac{\partial u_0}{\partial \theta} + \frac{w}{R}$$

$$\varepsilon_y^0 = \frac{\partial v_0}{\partial \theta}$$

$$\gamma_{y\theta}^0 = \frac{1}{R}\left(\frac{\partial v_0}{\partial \theta} + \frac{\partial u_0}{\partial y}\right) \tag{3.4}$$

$$\kappa_\theta = -\frac{1}{R^2}(w + \frac{\partial^2 w}{\partial \theta^2})$$

$$\kappa_y = -\frac{\partial^2 w}{\partial y^2}$$

$$\kappa_{\theta y} = \frac{2}{R}(\frac{\partial u_0}{\partial y} - \frac{\gamma_{\theta y}^0}{2} - \frac{\partial^2 w}{\partial y \partial \theta})$$

The first three terms of the equation 3.4 represent mid-plane strains and the last three terms represent the curvatures.

The Classical Lamination Plate Theory (CLPT) and the Classical Lamination Shell Theory (CLST) are the two theories that were primarily used to derive the mid-plane strains and curvature of the curved composite beams. These theories were very well discussed earlier by Chan with Demirham (1997), Chia (2007) and Mahadev (2015). Although these theories were analyzed for mechanical stresses and strains, The thermal terms are being included in this present work. The main difference between the CLPT and the CLST is the Curvature Factor $\left(1 + \frac{z''}{R_m}\right)$ of the cylindrical shell, which is used only in the Shell theory for calculating the Stiffness and the load matrices. Mahadev (2015) has stated that the influence of curvature factor plays a major role for closed section cylindrical shells, but in the case of open cross- sectional cylindrical shells, the error difference between the CLPT and CLST Stiffness matrices are negligible. In addition, the curvature factor has less effect compared to the plate theory for the larger radius. Hence, for a simple approach, we use the Classical Lamination Plate Theory for curved beams in our work.

In the laminated plate approach, an infinitesimal composite cylindrical plate element of a curved beam is rotated into a position which is parallel to the reference axis (as shown in

Figure 3.4). The rotated element is then translated to the reference axis. The stiffness of the beam is integrated by the element stiffness from the end of the beam to the other end.

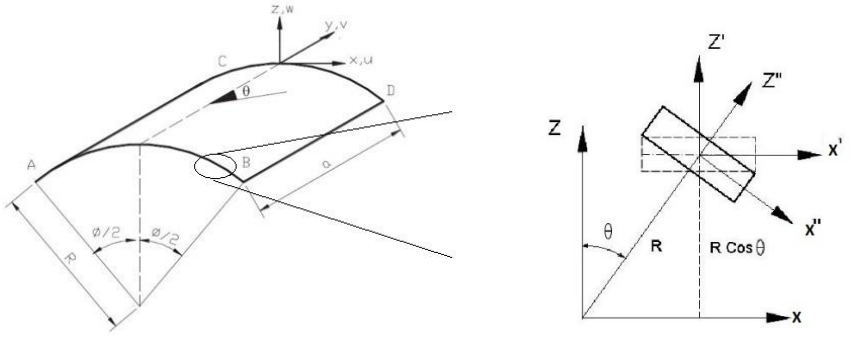

Figure 3.3 Plate rotated at angle θ

3.2.2.1 Transformation Matrices

The shell element is considered to be rotated at an angle θ with respect to the y axis and each ply is orientated at an angle β with respect to the z axis. Hence, it is vital to transform the matrices from the local coordinate system to the global coordinate system to obtain the material properties in the global coordinate system. Transformation of matrices should be accomplished for the Stiffness matrices and the Thermal coefficient of expansion matrices.

For θ Transformation about the y axis,

$$[T_\sigma]_y = \begin{bmatrix} m^2 & 0 & 0 \\ 0 & 1 & 0 \\ 0 & 0 & m \end{bmatrix} \tag{3.5}$$

$$[T_\varepsilon]_y = \begin{bmatrix} m^2 & 0 & 0 \\ 0 & 1 & 0 \\ 0 & 0 & m \end{bmatrix} \tag{3.6}$$

For β Transformation about z axis

$$[T_\sigma]_z = \begin{bmatrix} m^2 & n^2 & 2mn \\ n^2 & m^2 & -2mn \\ -mn & mn & m^2 - n^2 \end{bmatrix} \tag{3.7}$$

$$[T_\varepsilon]_z = \begin{bmatrix} m^2 & n^2 & mn \\ n^2 & m^2 & -mn \\ -2mn & 2mn & m^2 - n^2 \end{bmatrix}$$

Where m = cos θ, n = sin θ

The stiffness Matrix is transformed first about the z axis and then about the y axis.

$$[Q'] = [T_\sigma(-\beta)]_z[Q][T_\varepsilon(\beta)]_z \tag{3.8}$$

Then the Q' matrix is transformed about the y axis as follows.

$$\overline{[Q]}" = [T_\sigma(-\theta)]_y[Q'][T_\varepsilon(\theta)]_y \tag{3.9}$$

Similarly, the Coefficients of the thermal expansion are also transformed about the z axis and then the y axis as follows.

$$[\alpha'_{12}] = [T_\varepsilon(-\theta)]_z\,[\alpha_{12}] \tag{3.10}$$

$$[\alpha_{xy}] = [T_\varepsilon(-\theta)]_y\,[\alpha'_{12}] \tag{3.11}$$

3.2.2.2 Constitutive equation

Considering Nx", Ny", Nxy" as the applied resultant mechanical loads per unit width and Mx", My", Mxy" as the applied resultant moments per unit width acting on the composite tube differential element; axial, transverse and shear stresses can be associated to resultant force and moment components by

$$N"_x = \sum_{k=1}^{n}\int_{z_k}^{z_{k-1}} \sigma_x\ dz \qquad M"_x = \sum_{k=1}^{n}\int_{z_k}^{z_{k-1}} \sigma_x\ z"\ dz$$

$$N"_y = \sum_{k=1}^{n}\int_{z_k}^{z_{k-1}} \sigma_y\ dz \qquad M"_y = \sum_{k=1}^{n}\int_{z_k}^{z_{k-1}} \sigma_y\, z"\ dz \tag{3.12}$$

$$N"_{xy} = \sum_{k=1}^{n}\int_{z_k}^{z_{k-1}} \tau_{xy}\ dz \qquad M"_{xy} = \sum_{k=1}^{n}\int_{z_k}^{z_{k-1}} \tau_{xy}\ z"\ dz$$

Necessary assumption taken in regards about geometry of the composite tube is the existence of a uni-curvature around the circumference. The curvature is assumed to be absent along the y' plane as the tube span is extensively larger compared to tube mean radius. Furthermore, transverse shear stress effects are neglected since the laminate wall thickness assumed to be small.

The relation between the mechanical stress to strains in terms of the double transformed stiffness matrix can be given as

$$\begin{bmatrix}\sigma_x\\ \sigma_y\\ \tau_{xy}\end{bmatrix}_k = \begin{bmatrix}\overline{Q}"_{11} & \overline{Q}"_{12} & Q"_{16}\\ \overline{Q}"_{12} & \overline{Q}"_{22} & \overline{Q}"_{26}\\ \overline{Q}"_{61} & \overline{Q}"_{62} & \overline{Q}"_{66}\end{bmatrix} * \left[\begin{bmatrix}\varepsilon^{\circ}_X\\ \varepsilon^{\circ}_Y\\ \gamma^{\circ}_{XY}\end{bmatrix} + z * \begin{bmatrix}K_X\\ K_Y\\ K_{XY}\end{bmatrix} - \begin{bmatrix}\alpha_x\\ \alpha_y\\ \alpha_{xy}\end{bmatrix}_k * \Delta T\right] \quad (3.13)$$

Incorporating the mechanical stress from equation 3.13 into equation 3.12, we obtain

$$\begin{bmatrix}N"_x\\ N"_y\\ N"_{xy}\end{bmatrix} = \begin{bmatrix}A_{11} & A_{12} & A_{16}\\ A_{12} & A_{22} & A_{26}\\ A_{16} & A_{26} & A_{66}\end{bmatrix}\begin{bmatrix}\varepsilon^{\circ}_X\\ \varepsilon^{\circ}_Y\\ \gamma^{\circ}_{XY}\end{bmatrix} + \begin{bmatrix}B_{11} & B_{12} & B_{16}\\ B_{12} & B_{22} & B_{26}\\ B_{16} & B_{26} & B_{66}\end{bmatrix}\begin{bmatrix}K_X\\ K_Y\\ K_{XY}\end{bmatrix} - \begin{bmatrix}N^T_X\\ N^T_Y\\ N^T_{XY}\end{bmatrix} \quad (3.14)$$

$$\begin{bmatrix}M"_x\\ M"_y\\ M"_{xy}\end{bmatrix} = \begin{bmatrix}B_{11} & B_{12} & B_{16}\\ B_{12} & B_{22} & B_{26}\\ B_{16} & B_{26} & B_{66}\end{bmatrix}\begin{bmatrix}\varepsilon^{\circ}_X\\ \varepsilon^{\circ}_Y\\ \gamma^{\circ}_{XY}\end{bmatrix} + \begin{bmatrix}D_{11} & D_{12} & D_{16}\\ D_{12} & D_{22} & D_{26}\\ D_{16} & D_{26} & D_{66}\end{bmatrix}\begin{bmatrix}K_X\\ K_Y\\ K_{XY}\end{bmatrix} - \begin{bmatrix}M^T_X\\ M^T_Y\\ M^T_{XY}\end{bmatrix} \quad (3.15)$$

Equations 3.14 gives the resultant force deformation and equation 3.15 gives the moment deformation. Combining 3.14 and 3.15 we get equation 3.16

$$\begin{bmatrix}N"_x\\ N"_y\\ N"_{xy}\\ M"_x\\ M"_y\\ M"_{xy}\end{bmatrix} + \begin{bmatrix}N^T_X\\ N^T_Y\\ N^T_{XY}\\ M^T_X\\ M^T_Y\\ M^T_{XY}\end{bmatrix} = \begin{bmatrix}A_{11} & A_{12} & A_{16} & B_{11} & B_{12} & B_{16}\\ A_{12} & A_{22} & A_{26} & B_{12} & B_{22} & B_{26}\\ A_{16} & A_{26} & A_{66} & B_{16} & B_{26} & B_{66}\\ B_{11} & B_{12} & B_{16} & D_{11} & D_{12} & D_{16}\\ B_{12} & B_{22} & B_{26} & D_{12} & D_{22} & D_{26}\\ B_{16} & B_{26} & B_{66} & D_{16} & D_{26} & D_{66}\end{bmatrix}\begin{bmatrix}\varepsilon^{\circ}_X\\ \varepsilon^{\circ}_Y\\ \gamma^{\circ}_{XY}\\ K_X\\ K_Y\\ K_{XY}\end{bmatrix} \quad (3.16)$$

In our analysis, we only have the thermal forces and moment, and no mechanical forces or moments. Hence we can remove N" and M" terms. Hence equation 3.16 becomes

$$\begin{bmatrix}N^T_X\\ N^T_Y\\ N^T_{XY}\\ M^T_X\\ M^T_Y\\ M^T_{XY}\end{bmatrix} = \begin{bmatrix}A_{11} & A_{12} & A_{16} & B_{11} & B_{12} & B_{16}\\ A_{12} & A_{22} & A_{26} & B_{12} & B_{22} & B_{26}\\ A_{16} & A_{26} & A_{66} & B_{16} & B_{26} & B_{66}\\ B_{11} & B_{12} & B_{16} & D_{11} & D_{12} & D_{16}\\ B_{12} & B_{22} & B_{26} & D_{12} & D_{22} & D_{26}\\ B_{16} & B_{26} & B_{66} & D_{16} & D_{26} & D_{66}\end{bmatrix}\begin{bmatrix}\varepsilon^{\circ}_X\\ \varepsilon^{\circ}_Y\\ \gamma^{\circ}_{XY}\\ K_X\\ K_Y\\ K_{XY}\end{bmatrix} \quad (3.17)$$

Equation 3.17 gives constitutive equation for the curved beam element as per CLPT.

Where the terms are given below in 3.18,

$$[A] = \sum_{k=1}^{n} \int_{z_k}^{z_{k-1}} \overline{\left[Q"_{xy}\right]_k}\, dz = \sum_{k=1}^{n} \overline{\left[Q"_{xy}\right]_k} (z_k - z_{k-1})$$

$$[B] = \sum_{k=1}^{n} \int_{z_k}^{z_{k-1}} \overline{\left[Q"_{xy}\right]_k}\, z\, dz = \frac{1}{2} \sum_{k=1}^{n} \overline{\left[Q"_{xy}\right]_k} ({z^2}_k - {z^2}_{k-1})$$

$$[D] = \sum_{k=1}^{n} \int_{z_k}^{z_{k-1}} \overline{\left[Q"_{xy}\right]_k}\, z^2\, dz = \frac{1}{3} \sum_{k=1}^{n} \overline{\left[Q"_{xy}\right]_k} ({z^3}_k - {z^3}_{k-1})$$

$$[N^T] = \sum_{k=1}^{n} \int_{z_k}^{z_{k-1}} \overline{\left[Q"_{xy}\right]_k} * \left[\alpha_{xy}\right]_k * \Delta T\, dz = \sum_{k=1}^{n} \overline{\left[Q"_{xy}\right]_k} * \left[\alpha_{xy}\right]_k * \Delta T\ (z_k - z_{k-1})$$

$$[M^T] = \sum_{k=1}^{n} \int_{z_k}^{z_{k-1}} \overline{\left[Q"_{xy}\right]_k} * \left[\alpha_{xy}\right]_k * \Delta T * z\, dz = \frac{1}{2} \sum_{k=1}^{n} \overline{\left[Q"_{xy}\right]_k} * \left[\alpha_{xy}\right]_k * \Delta T\ (z_k - z_{k-1})$$

3.2.2.3 Constitutive Equation for the Curved Beam Element in Global System

To transform the element stiffness matrices and force, moment terms to the global coordinate system, two steps are being followed. First, the terms are implemented in the parallel axes theorem and next they are being integrated over the entire circumference of the tube for the infinitesimal element.

Hence by Parallel Axes Theorem, the stiffness matrices are

$$\left[\hat{A}\right] = [A]$$

$$\left[\hat{B}\right] = [B] + R_m * \cos\theta * [A] \tag{3.19}$$

$$\left[\widehat{D}\right] = [D] + 2 * R_m * \cos\theta * [B] + (R_m * \cos\theta)^2 * [A]$$

By Parallel Axes Theorem, the force matrices are

$$\left[\widehat{N^T}\right] = [N^T]$$

$$\left[\widehat{M^T}\right] = [M^T] + R_m * \cos\theta * [N^T] \tag{3.20}$$

Next by integrating the elements over the entire circumference, we obtain,

$$\overline{[A]} = \int_{\alpha}^{-\alpha}\left[\hat{A}\right] * R_m * d\theta \qquad \overline{[N^T]} = \int_{\alpha}^{-\alpha}\left[\widehat{N^T}\right] * R_m * d\theta$$

$$\overline{[B]} = \int_{\alpha}^{-\alpha}\left[\hat{B}\right] * R_m * d\theta \qquad \overline{[M^T]} = \int_{\alpha}^{-\alpha}\left[\widehat{M^T}\right] * R_m * d\theta \tag{3.21}$$

$$\overline{[D]} = \int_{\alpha}^{-\alpha}\left[\hat{D}\right] * R_m * d\theta$$

Substituting the global stiffness and force terms into equation 3.17, we obtain the global constitutive equation. The Mid-Plane strains and curvature terms are obtained from it, and the strain components, deformation, and in-plane stress can be calculated

$$\begin{Bmatrix} \varepsilon''_o \\ \kappa''_o \end{Bmatrix} = \begin{bmatrix} \bar{a} & \bar{b} \\ \overline{b^T} & \bar{d} \end{bmatrix}_{6*6} * \begin{Bmatrix} \bar{N} \\ \bar{M} \end{Bmatrix}_{6*1} \tag{3.23}$$

Where $\bar{a},\ \bar{b}\ and\ \bar{d}$ are the global compliance matrices related with a thin-walled cylindrical composite tube, obtained by a direct inversion of the 6*6 global stiffness matrices.

3.2.2.4 In-Plane Stress calculation

The total strain of each ply is obtained using mid-plane strain and curvature, multiplied by the ply coordinate. Then, the mechanical strain is obtained by subtracting the thermal strain from the total strain of each ply. Finally, the ply stress can be obtained from product of the stiffness matrix of that ply and the mechanical strain. The ply stress is expressed as below

$$\left[\varepsilon_{x-y}^{Total}\right]_k = [\varepsilon^0] + (R + z').cos\theta.[\kappa]$$

$$[\varepsilon_{x-y}^{M}]_k = [\varepsilon_{x-y}^{Total}]_k - [\alpha_{x-y}]_k.\Delta T \tag{3.24}$$

$$[\sigma_{x-y}]_k = [\widehat{Q}]_k.[\varepsilon_{x-y}^{M}]_k$$

3.3 Finite Element Modelling of Curved Beam

The same material properties, element type and layup of the laminates were used that was discussed in Chapter 2.

3.3.1 Development of 2D - Finite Element Model of Curved Beam

For 2D Modelling, a curved shell was modelled. The element type was chosen as SHELL281. As it was a composite layup, the storage of layer data K8 value was set to All Layers in the options. The Shell section is defined as in Chapter 2.

Modelling of the Curved Beam

A curved area is created with the inner radius of 2 inches and angle of 30 degrees. The width of the curved shell is 0.25 inches.

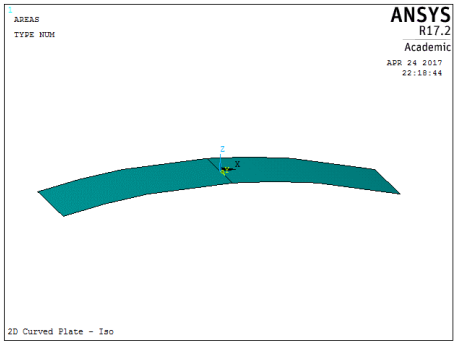

Figure 3.4 2-D Model of the Curved shell

Meshing

The meshing was performed by defining the line element size as required along the breadth and width of the curved area. Line element size was set in such a way that the ratio of thickness of element to any other dimension of element is not 1:10. The line element size was determined by mesh convergence criteria.

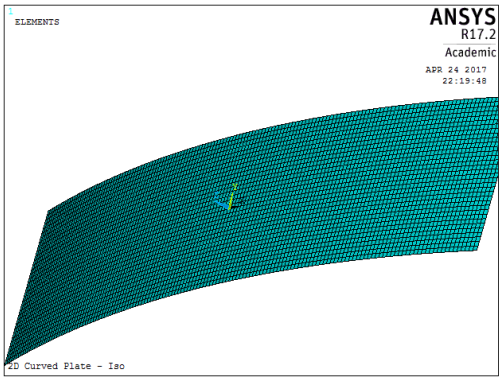

Figure 3.5 Mesh of the Curved Beam

Boundary and Loading Conditions

ANSYS requires the structure to be fixed. Hence the center (0,0) was constrained in all degrees of freedom, so that there will be no transitional motion and no rotational motion at origin on x, y and z-direction. (Ux = Uy = Uz = 0). A uniform temperature load of 172 °F was applied, such that difference between load temperature and room temperature was 100°F. The model was solved.

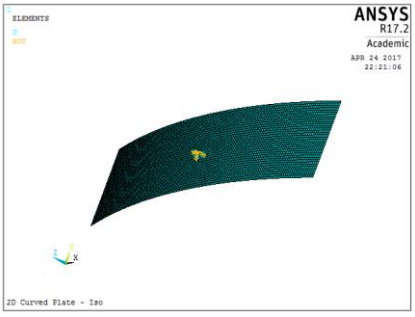

Figure 3.6 Loading Conditions for the 2D Curved Shell

For thickness option, the element view can be selected in options and plate can be viewed along thickness.

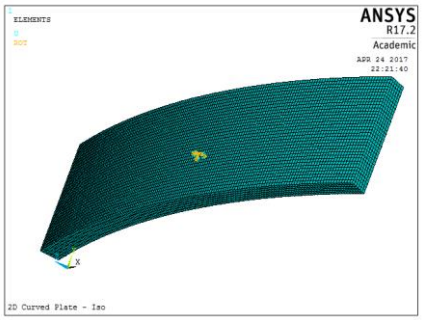

Figure 3.7 Curved Shell with Thickness Option

Post Processing

The X, Y and Z component of deformation are obtained for each model. As it is a curved shell, the 4 nodal points which are the four corners of the curved shell are taken into consideration for comparison with the theoretical values.

3.3.2 Development of 3D- Finite Element Model of Curved Beam

To study the thickness variation of the curvature due to thermal load, and to include the third dimensional properties in the calculations, a 3D solid model of curved beam is being created layer by layer. This will produce more accurate results than the 2D model, as in the 2D analytical and FEM Models, the strain in z-direction is being ignored. The same SOLID186 element was used as in laminates.

Modelling of the 3D Curved Beam

The curved beam was created by creating areas on the x-y plane and rotating it around z-axis to form volumes. The additional volumes were deleted to obtain a curved beam of 30 degrees. In the SOLID Model, each layer of curved beam is of different lengths. The Element orientation for each layer is given by creating local coordinates.

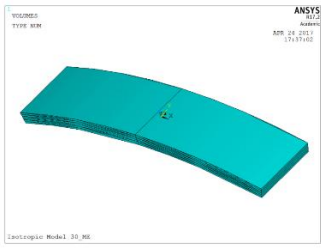

Figure 3.8 3D – Curved Beam

Meshing

Each ply is meshed individually with respects to its material orientation. Each line of the volume is being selected and the line element size was defined. Since it is a composite laminate, the line element size for Z- direction line is always 1, as the composite plies are not split into elements in the thickness direction. Once the volume attributes and the line element attributes are defined, the volume is meshed. Similar procedure is repeated for all the plies. Curved lamina mesh and curved laminate mesh are shown in following Figure 3.9

Figure 3.9 Mesh of Curved Laminates

Boundary and Loading Conditions

For the case of 2D curved shell element, the model was fixed at the center of reference. But for the 3-D solid elements, fixing it only at the center of the plate makes it less constrained. Hence the model was fixed in center of origin in all directions (UX = 0 ; UY = 0 ; UZ = 0) and also the nodes through the thickness direction of the center element (x = 0 ; y = 0 ; z varies) was constrained in the X and Y directions (UX = 0 ; UY = 0) . Also, the temperature load of 172 °F

was being applied with the room temperature set to 72 °F. Hence a temperature difference of 100°F is obtained. The model is solved.

The boundary conditions are shown in Figure 3.10.

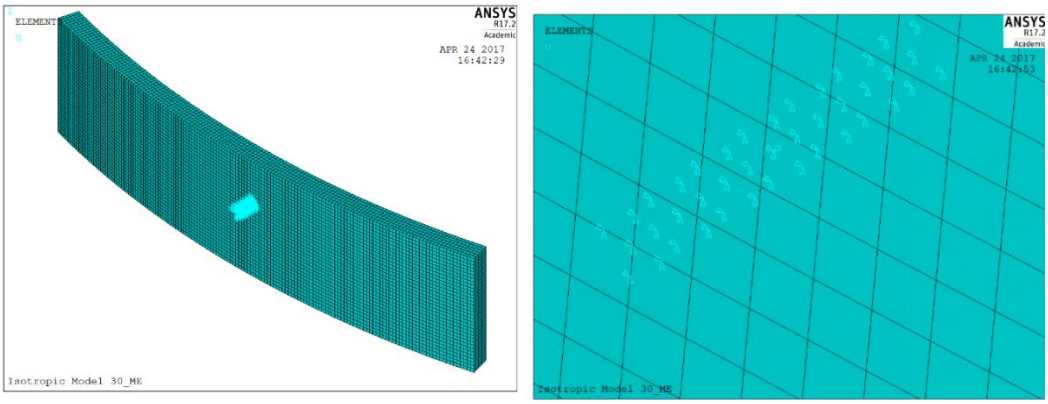

Figure 3.10 Boundary Conditions for a 3-D Model

Post Processing

Certain nodal points are selected where the displacement is needed to be calculated. The z component of deformation is calculated at these points, and the change in the thickness of the element is computed. The nodal points which are selected for calculation are shown in Figure 3.11

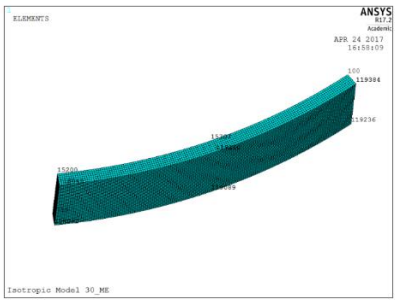

Figure 3.11 Nodes for Obtaining Results

3.3.2.1 Mesh Convergence

The Importance of mesh convergence was discussed in detail in Chapter 2. The same methodology was repeated to determine the finer mesh model for the curved beam. The Number of elements was increased by varying the element size of the length and breadth of the

curved beam. The line element size along the thickness direction was always 1. The Displacement values were obtained at the inner surface of the curved beam edge.

Model	Ratio L : B : H	No. of Nodes	No. of elements	U_{sum} at Node selected	Error %
A	16 : 12 : 1	1373	240	7.3036E-4	-
B	8 : 6 : 1	3409	648	7.4808E-4	2.37
C	4 : 3 : 1	12637	2592	7.5395E-4	0.78
D	2 : 1 : 1	70105	15096	7.5558E-4	0.22
E	1: 1: 1	139517	29784	7.5594E-4	0.05

Table 3.2 Mesh Convergence for 3D Curved Beam

3.3.2.2 Validation of the 3-D Finite Element Model of curved beam

The 3-D finite element model which is created was first validated by using the isotropic material properties. Aluminum AL6061-T6 was chosen as the isotropic material and its properties were used. The properties of the aluminum are

$$E = 10 \text{ Msi} ; v = 0.33 ; \alpha = 14 \times 10^{-6} ; G = 3.75 \text{ Msi}$$

The Deformations in X, Y, Z directions were obtained from the Finite Element Model and compared with the Analytical Solutions.

Deformation of an Curved Beam – 3D Finite element model

The X, Y, Z and total components of deformation of the 3D Curved Beam is shown in Figures 3.13. The Change in length is calculated by selecting the nodal points of the line and calculating through its deformations.

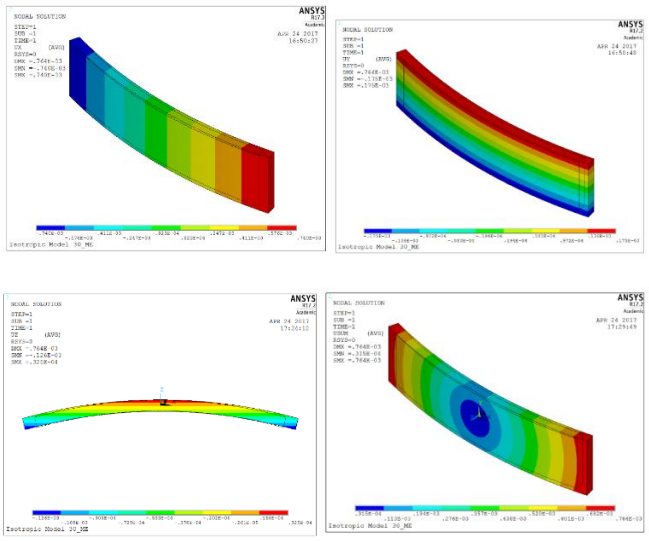

Figure 3.12 Top Right, Top Left, Bottom Right, Bottom Left – represents X, Y, Z and Total Deformation of Isotropic Curved Beam respectively

Results

The analytical and finite element results are compared in the following Table. The Deformation value is obtained at the inner radius of the curved beam

Table 3.3 Analytical and Finite Element Deformations of the Isotropic Plate

	Initial Length (inches)	Change in Length (dl) Analytical	Change in Length 2D FEM	Change in Length 3D FEM	3D - Error %
X (Breadth)	1.0472	1.466E-4	1.466E-4	1.449E-4	2.22 %
Y (Height)	0.25	0.35E-4	0.35E-4	0.35E-4	0 %
Z (Thickness)	0.0432	0.6048E-4	0.6048E-4	0.5836E-4	2.50 %

Since the error percentages are very negligible, the finite element results agree with the theoretical results. Hence this 3-D model can be used for calculating the deformations of the composite curved beams.

Chapter 4

RESULTS AND DISCUSSIONS

In the previous chapter 2 and 3, we had the derived the deformation of the composite laminates and curved beams by both analytical and finite element model. This chapter verifies the results of the analytical and finite element method, and studies the change of thickness of the plate and curved beams due to the thermal loads.

4.1 Laminates

4.1.1 Nodal Points (NP)

For comparing the results, four points at the corners are the plates are chosen, and the deformation at those points are being obtained.

Table 4.1 Points where deflection is obtained

Point	X	Y
1	-1	-0.75
2	1	-0.75
3	1	0.75
4	-1	0.75

4.1.2 Plate A – Symmetric Balanced Laminate

The deformation of plate A is given by Equations 2.31 and 2.32 from Chapter 2. These deformations are compared with the deformations obtained from the 2-D finite element modelling.

Table 4.2 X and Y Deformations of Plate A

	Analytical Results (in)		FEA Results (in)		Deformation in X	Deformation in Y
NP	U_0	V_0	UX	UY	Error %	Error %
1	0.1459E-4	-0.3076E-3	0.1459E-4	-0.3076E-3	0 %	0 %
2	-0.1459E-4	-0.3076E-3	-0.1459E-4	-0.3076E-3	0 %	0 %
3	-0.1459E-4	0.3076E-3	-0.1459E-4	0.3076E-3	0 %	0 %
4	0.1459E-4	0.3076E-3	0.1459E-4	0.3076E-3	0 %	0 %

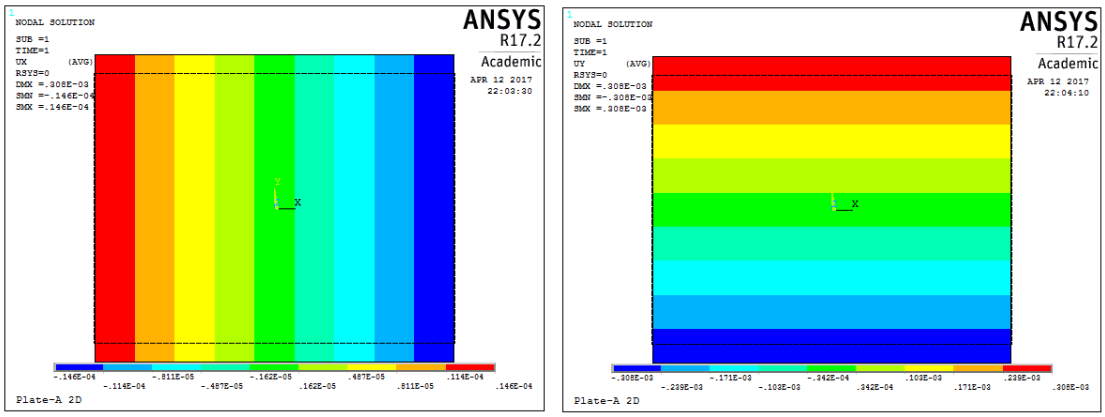

Figure 4.1 X and Y Component of Deformation of Plate A

Since the Z component of deformation cannot be obtained from 2-D model, the 3-D model was used to study the deformation in the Z direction. The thickness change is also evaluated from FEM model.

The Z component of deformation varies based on X and Y Locations. The actual thickness of plate is 0.0432 inch.

Table 4.3 Z component of Deformation and Thickness Change - A

Nodal Location				
X (in)	Y (in)	Z (in)	Deformation in Z (in)	Change in thickness (in)
1	0.75	-0.0216	-5.9567E-5	1.1913E-4
1	0.75	0.0216	5.9568E-5	
1	-0.75	-0.0216	-2.3353E-5	0.4670E-4
1	-0.75	0.0216	2.3353E-5	
-1	-0.75	-0.0216	-5.9567E-5	1.1913E-4
-1	-0.75	-0.0216	5.9567E-5	
-1	0.75	-0.0216	-2.3353E-5	0.4670E-4
-1	0.75	0.0216	2.3353E-5	

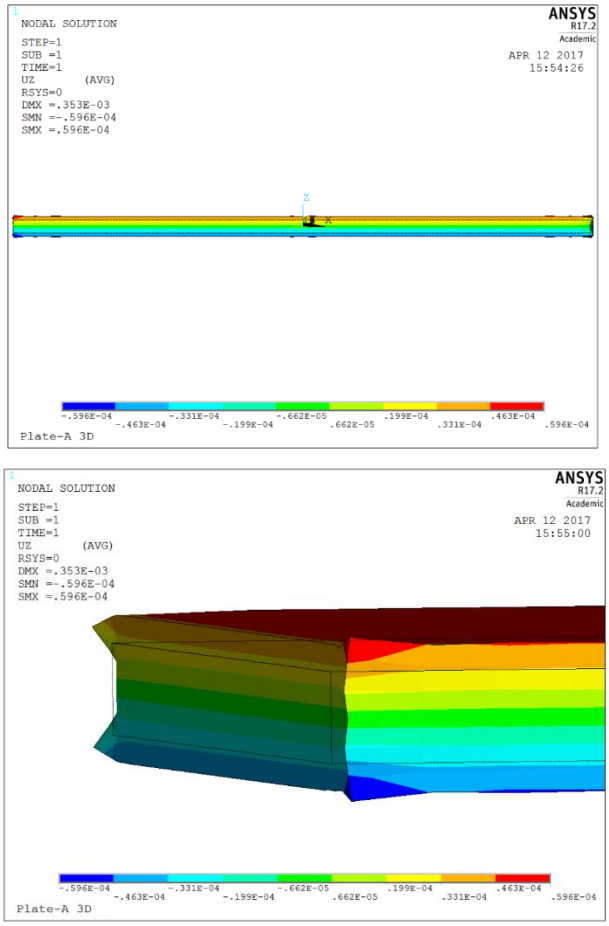

Figure 4.2 Z and In Detailed - Z Component of Deformation of Plate A

4.1.3 Plate B – Symmetric Unbalanced Laminate

The deformation of Plate B is given by Equations 2.36 and 2.37 from Chapter 2. These deformations are compared with the deformations obtained from the 2-D finite element modelling.

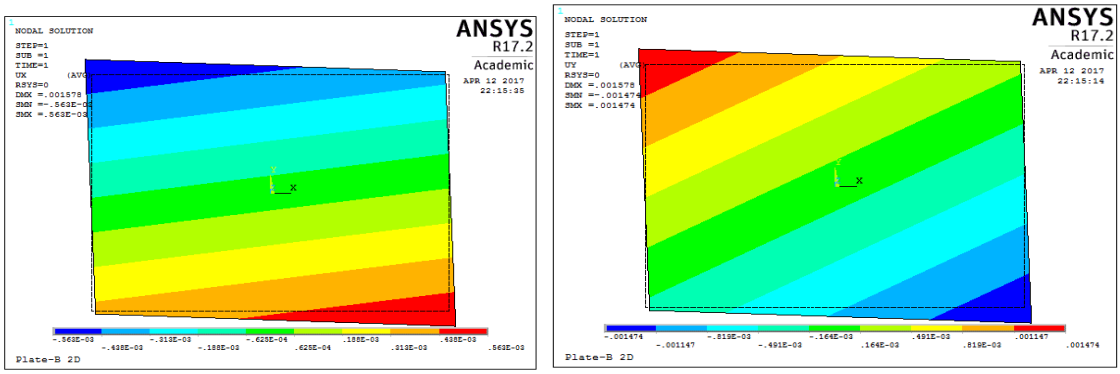

Figure 4.3 X and Y Component of Deformation of Plate B

Table 4.4 X and Y Deformations of Plate B

	Analytical Results (in)		FEA Results (in)		Deformation in X	Deformation in Y
	U_0	V_0	UX	UY	Error %	Error %
1	0.3579E-3	-0.2462E-3	0.3579E-3	-0.2462E-3	0.0004 %	0.00067 %
2	0.5629E-3	-1.4741E-3	0.5629E-3	-1.4742E-3	0.00002 %	0 %
3	-0.3579E-3	0.2462E-3	-0.3579E-3	0.2462E-3	0.0004 %	0.00067 %
4	-0.5629E-3	1.4741E-3	-0.5629E-3	1.4742E-3	0.00002 %	0 %

Since the Z component of deformation cannot be obtained from 2-D model, the 3-D Model was used to study the deformation in the Z direction. The thickness change is also evaluated from FEM Model.

The Z component of deformation varies based on X and Y Locations.

Table 4.5 Z component of Deformation and Thickness Change - B

Nodal Location				
X (in)	Y (in)	Z (in)	Deformation in Z (in)	Change in thickness (in)
1	0.75	-0.0216	-4.056E-5	0.8113E-4
1	0.75	0.0216	4.056E-5	
1	-0.75	-0.0216	-3.022E-5	0.6045E-4
1	-0.75	0.0216	3.022E-5	
-1	-0.75	-0.0216	-4.056E-5	0.8113E-4
-1	-0.75	-0.0216	4.056E-5	
-1	0.75	-0.0216	-3.022E-5	0.6045E-4
-1	0.75	0.0216	3.022E-5	

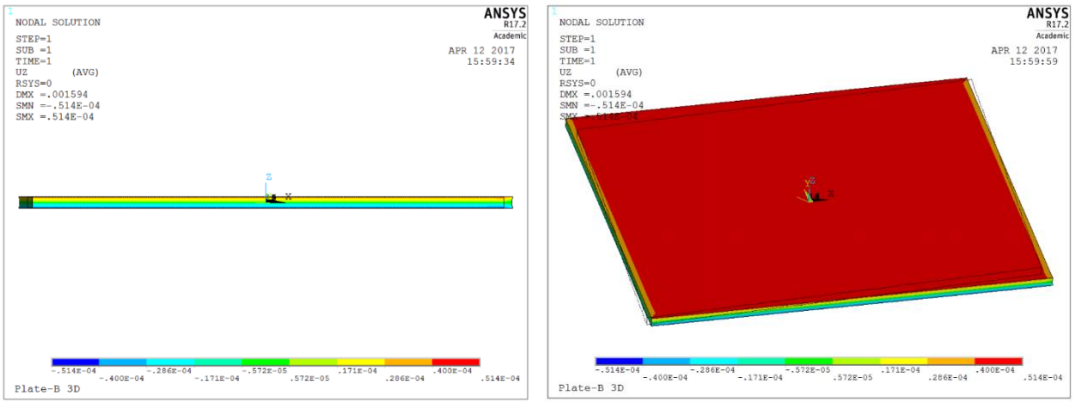

Figure 4.4 Z and In Detailed - Z Component of Deformation of Plate B

From the results of plate A and plate B, which are both symmetrical laminates, we can observe that the deformation in the X, Y and Z direction are also symmetrical in manner.

4.1.4 Plate C – Un-Symmetric Balanced Laminate

As discussed in chapter two, the un-symmetric laminates have curvature, and hence the Z-component of deformation exists in both 2D and 3D plates. Hence a better comparison was obtained with the 2D and 3D finite element results.

Table 4.6 Analytical and FEA Deformation of Plate C

	Analytical Results (in)			FEA Results (in)		
NP	U_0	V_0	W_0	UX	UY	UZ
1	-2.9483E-5	-3.7491E-4	-7.2785E-3	-0.2948E-4	-0.3749E-3	-0.7278E-2
2	-2.2583E-5	-3.0549E-4	2.7164E-3	-0.2258E-4	-0.3054E-3	0.2716E-2
3	2.9483E-5	3.7491E-4	-7.2785E-3	0.2948E-4	0.3749E-3	-0.7278E-2
4	2.2583E-5	3.0549E-4	2.7164E-3	0.2258E-4	0.3054E-3	0.2716E-2

Table 4.7 Error % for Deformations in Plate C

Deformation in X	Deformation in Y	Deformation in Z
Error %	Error %	Error %
0.013 %	0.0026 %	0 %
0.0031 %	0 %	0.0011 %
0.013 %	0.0026 %	0 %
0.0031 %	0 %	0.0011 %

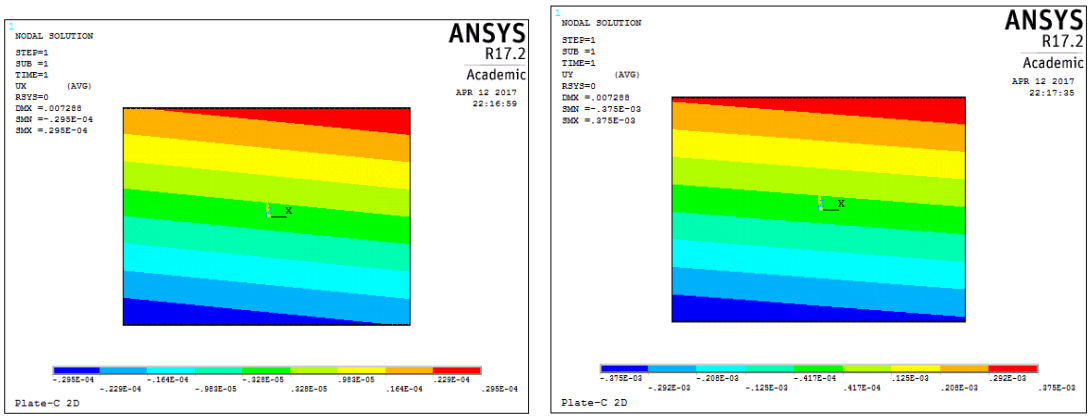

Figure 4.5 X and Y Component of Deformation in Plate C

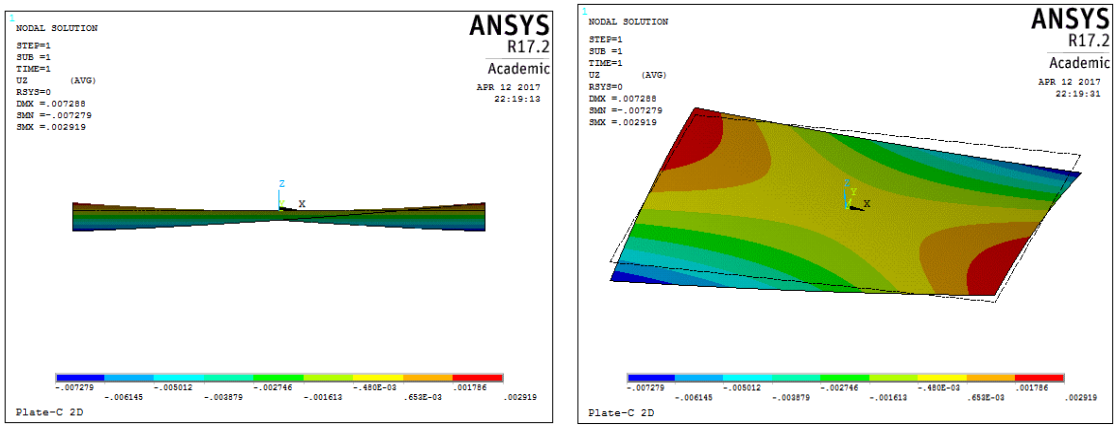

Figure 4.6 Z component Deformation in 2D – Plate C

For more accurate values of the Z – component deformation and the thickness change of the plate, the results from the 3D FEA model are shown in the below Table.

The results from Table 4.8 clearly indicates that the thickness of the unsymmetrical balanced laminate changes in each corner and are found to be the same in opposite corners. The deformation values in Z direction indicates that the laminate curves upwards in opposite corners and downwards in the other two corners.

Table 4.8 3D – Z Component of Deformation

Nodal Point Location			Analytical Results (in)	3D FEA results (in)	Error %	Change in thickness (in)
X (in)	Y (in)	Z (in)				
1	0.75	-0.0216	-7.2785E-3	-7.4112E-3	1.82 %	0.831E-4
1	0.75	0.0216		-7.4943E-3	2.96 %	
1	-0.75	-0.0216	2.7164E-3	2.8279E-3	4.10 %	0.619E-4
1	-0.75	0.0216		2.7660E-3	1.82 %	
-1	-0.75	-0.0216	-7.2785E-3	-7.4112E-3	1.82 %	0.831E-4
-1	-0.75	-0.0216		-7.4943E-3	2.96 %	
-1	0.75	-0.0216	2.7164E-3	2.8279E-3	4.10 %	0.619E-4
-1	0.75	0.0216		2.7660E-3	1.82 %	

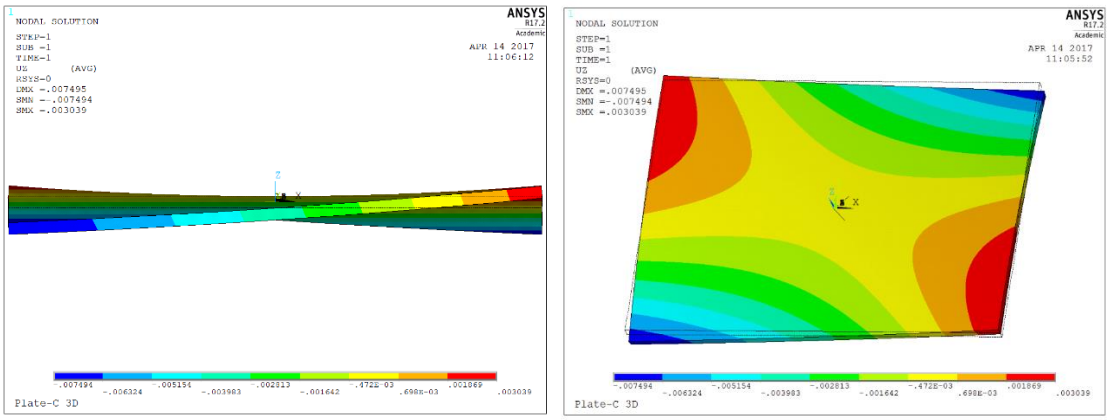

Figure 4.7 Z component deformation of the 3D Plate C – (Side and Top View)

4.1.5 Plate D – Un-Symmetrical Un-Balanced Laminate

In the previous section, un-symmetrical balanced laminate was studies. In this section, we will discuss how the Z component of deformation varies for an un-symmetrical and un-balanced laminate. The analytical results are obtained from equations 2.29, 2.30 and 2.31.

Table 4.9 Analytical and FEA Deformation of Plate D

	Analytical Results (in)			FEA Results (in)		
NP	U_0	V_0	W_0	UX	UY	UZ
1	3.1510E-4	-0.2286E-3	-0.3574E-3	0.3151E-3	-0.2286E-3	-0.3574E-3
2	6.1892E-4	-1.473E-3	6.358E-3	0.6189E-3	-1.474E-3	6.3584E-3
3	-3.1510E-4	0.2286E-3	-0.3574E-3	-0.3151E-3	0.2286E-3	-0.3574E-3
4	-6.1892E-4	1.473E-3	6.358E-3	-0.6189E-3	-1.474E-3	6.3584E-3

Table 4.10 Error % for Deformations in Plate D

Deformation in X	Deformation in Y	Deformation in Z
Error %	Error %	Error %
0.0009 %	0.0013 %	0.0025 %
0.0008 %	0.067 %	0.0062 %
0.0009 %	0.0013 %	0.0025 %
0.0008 %	0.067 %	0.0062 %

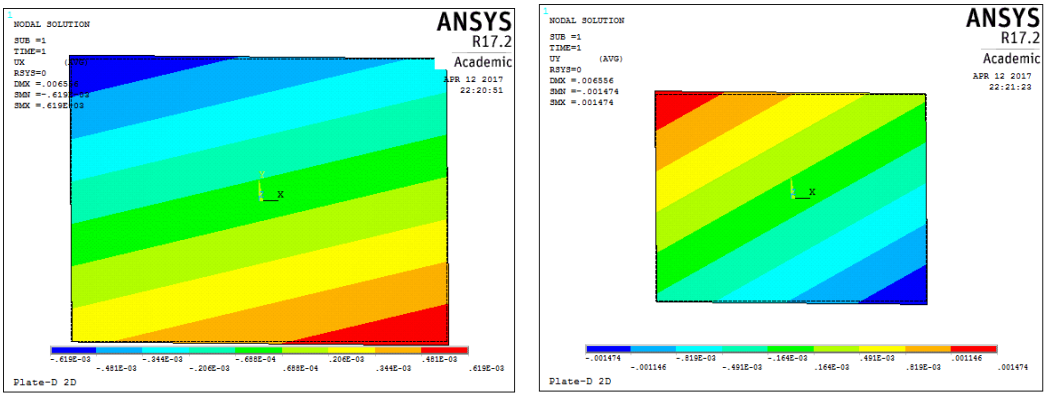

Figure 4.8 X and Y Component of Deformation in Plate D

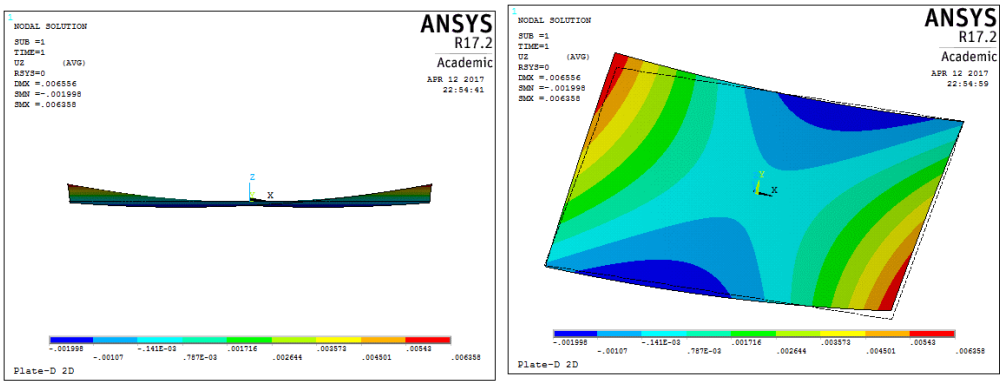

Figure 4.9 Z component Deformation in 2D – Plate D

For more accurate values of the Z – component deformation and the thickness change of the plate, the results from the 3D FEA model are shown in the below Table.

Table 4.11 3D – Z Component of Deformation – Plate D

Nodal Point Location			Analytical Results (in)	3D FEA results (in)	Error %	Change in thickness (in)
X(in)	Y(in)	Z(in)				
1	0.75	-0.0216	-0.3574E-3	-0.3160E-3	10.42 %	0.6465E-4
1	0.75	0.0216		-0.3806E-3	6.49 %	
1	-0.75	-0.0216	6.358E-3	6.4653E-3	1.68 %	0.7460E-4
1	-0.75	0.0216		6.3907E-3	0.51 %	
-1	-0.75	-0.0216	-0.3574E-3	-0.3160E-3	10.42 %	0.6465E-4
-1	-0.75	-0.0216		-0.3806E-3	6.49 %	
-1	0.75	-0.0216	6.358E-3	6.4653E-3	1.68 %	0.7460E-4
-1	0.75	0.0216		6.3907E-3	0.51 %	

The results from the above Table 4.11 indicate higher error values for results observed from two corners for the 2D and 3D model, but a similar pattern and range of values are observed for 2D and 3D models and the overall results for the other two corners, the results obtained for other laminates, proves that the 3D model is accurate. From the above results, the un-symmetrical un-balanced laminate has the thickness change and curvature similar in the opposite corners of the plate.

From the overall results of all the laminates, it can be concluded that the thickness variation is not uniform due to the thermal load, and it follows a symmetric pattern over the diagonal length of the plate. Hence, more accurate conclusion can be given by studying on the square plates and by varying the dimensions for the rectangular plates.

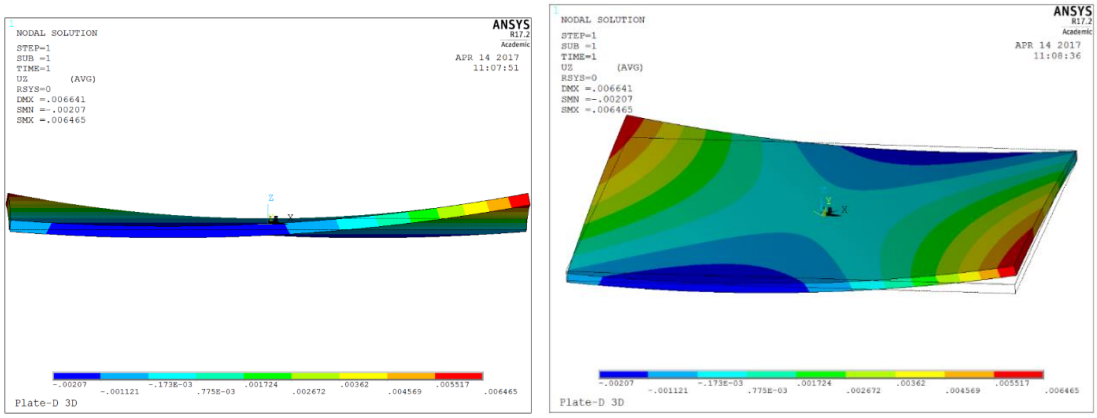

Figure 4.10 Z component Deformation of the 3D Plate D (Side and Top View)

4.2 Curved Beams

4.2.1 Stresses at Node

From the theoretical solution of curved beams, the stress value is obtained for the laminate top layer, at an angle of 15 degree and Y = 0. The stress value is obtained as per equation 2.32. The values are compared and verified with the 2D and 3D finite element model to prove the model. Later the deformation in Z direction and change in thickness for the 3D finite element model is studied.

4.2.2 Curved Beam A – Symmetric Balanced Layup

The stressed from the analytical and FEM models for a symmetric balanced layup of composite curved beam is given in the following Table. The layup sequence is $[45 / -45 / 0]_S$.

Stress (psi)	Analytical	2D FEM	3D FEM
σ_X	450.79	451.21	450.36
σ_Y	1081.9	1080.6	1081.2
γ_{XY}	3186.4	3191.5	3187.8

Table 4.12 Stress Comparison for Curved Beam A

The deformation in X, Y and Z component for the 3D curved beam A is shown in Figure 4.11.

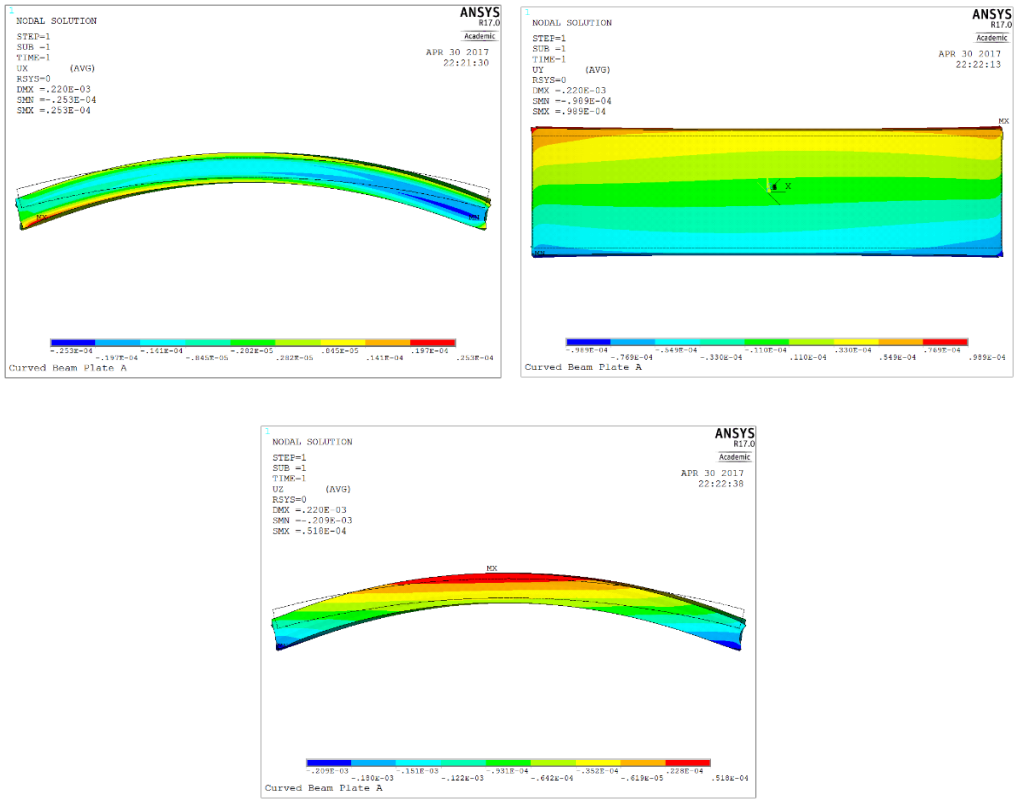

Figure 4.11 X, Y and Z Component Deformation for Curved Beam A

4.2.3 Curved Beam B – Symmetric Un-Balanced Layup

The stressed from the Analytical and FEM models for a symmetric un-balanced layup of composite curved beam is given in the following Table. The layup sequence is [45 / 45 / 0]$_S$.

Stress (psi)	Analytical	2D FEM	3D FEM
σ_X	-1112.1	-1117.5	-1113.32
σ_Y	453.37	453.07	453.24
γ_{XY}	462.43	461.88	462.58

Table 4.13 Stress Comparison for Curved Beam B

The deformation in X, Y and Z component for the 3D curved beam B is shown in Figure 4.12.

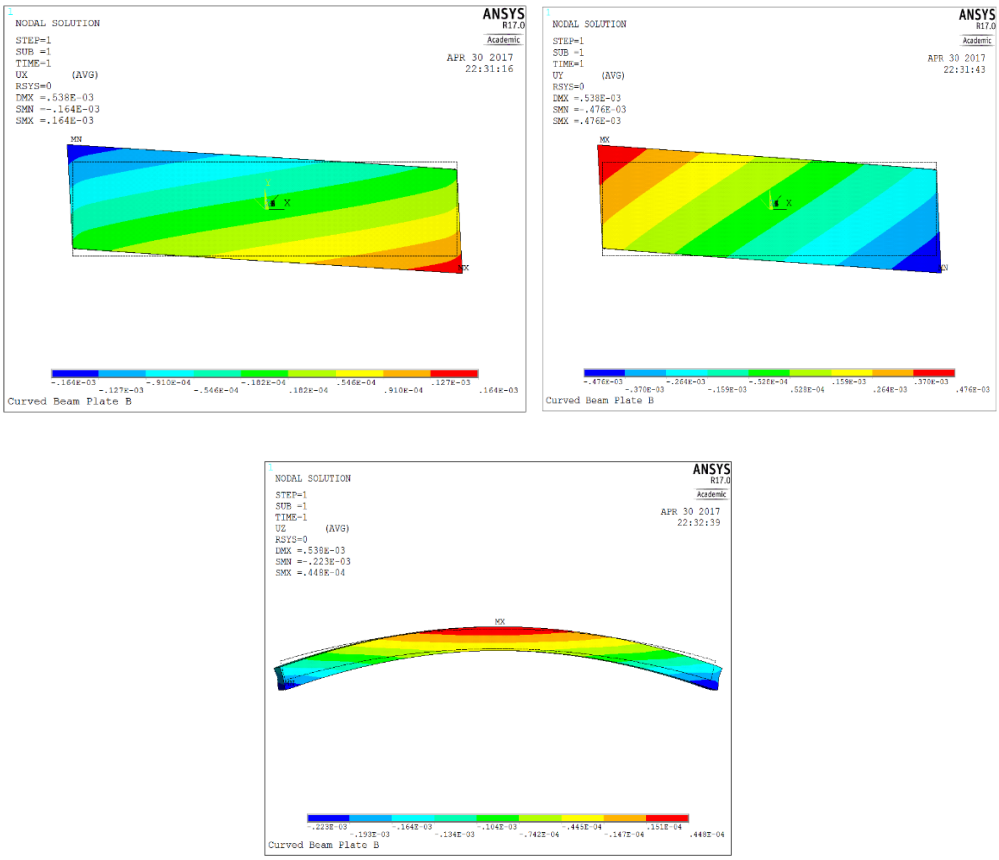

Figure 4.12 X, Y and Z Component Deformation for Curved Beam B

4.2.4 Curved Beam C – Un-Symmetric Balanced Layup

The stressed from the analytical and FEM models for an un-symmetric balanced layup of curved beam is given in the following Table. The layup sequence is $[\ 45 / -45 / 0\ ]_{2T}$.

Stress (Psi)	Analytical	2D FEM	3D FEM
σ_X	-1023.7	-1025.3	-1023.6
σ_Y	-1724.0	-1724.6	-1725.9
γ_{XY}	268.1	267.6	267.3

Table 4.14 Stress Comparison for Curved Beam C

The deformation in X, Y and Z component for the 3D curved beam C is shown in Figure 4.13.

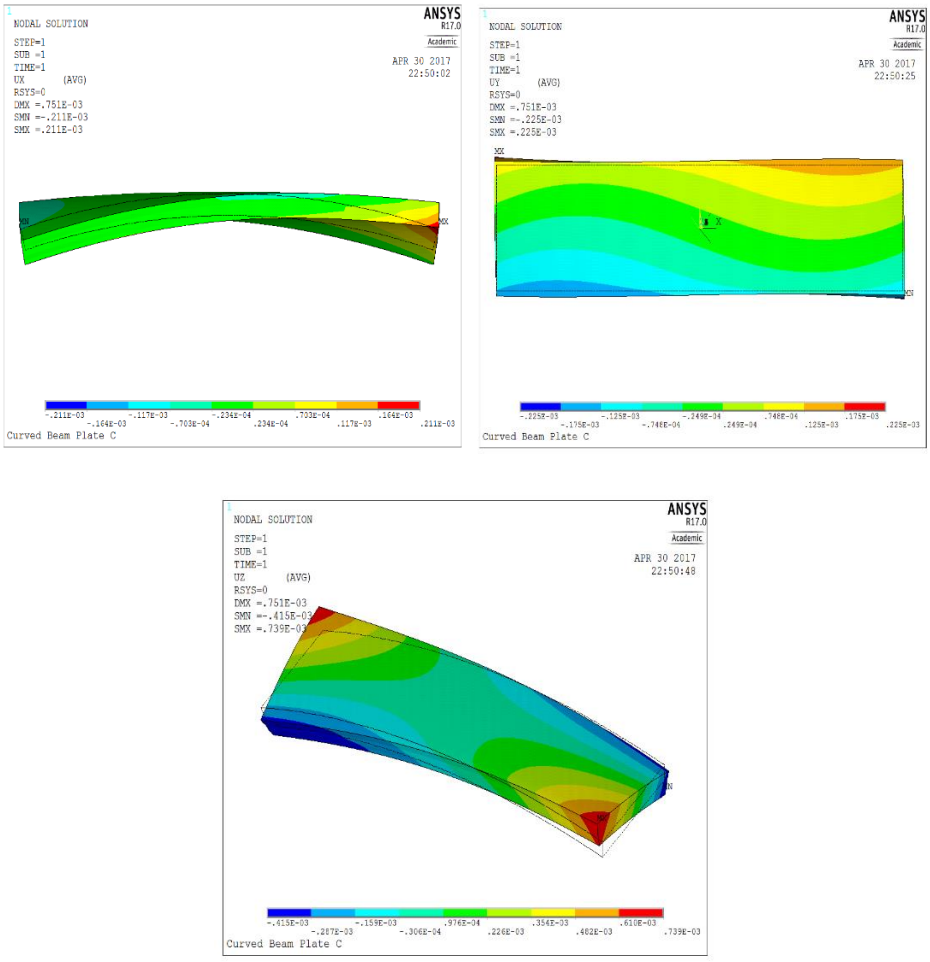

Figure 4.13 X, Y and Z Component Deformation for Curved Beam C

4.2.5 Curved Beam D – Un-Symmetric Un-Balanced Layup

The stressed from the analytical and FEM Models for an un-symmetric un-balanced layup of composite curved beam is given in the following Table. The layup sequence is [45 / 45 / 0]$_{2T}$.

Stress (psi)	Analytical	2D FEM	3D FEM
σ_X	-1183.6	-1179.3	-1182.5
σ_Y	-152.1	-151.2	-151.8
γ_{XY}	-139.2	-139.4	-138.6

Table 4.15 Stress Comparison for Curved Beam D

The deformation in X, Y and Z component for the 3D curved beam D is shown in Figure 4.14.

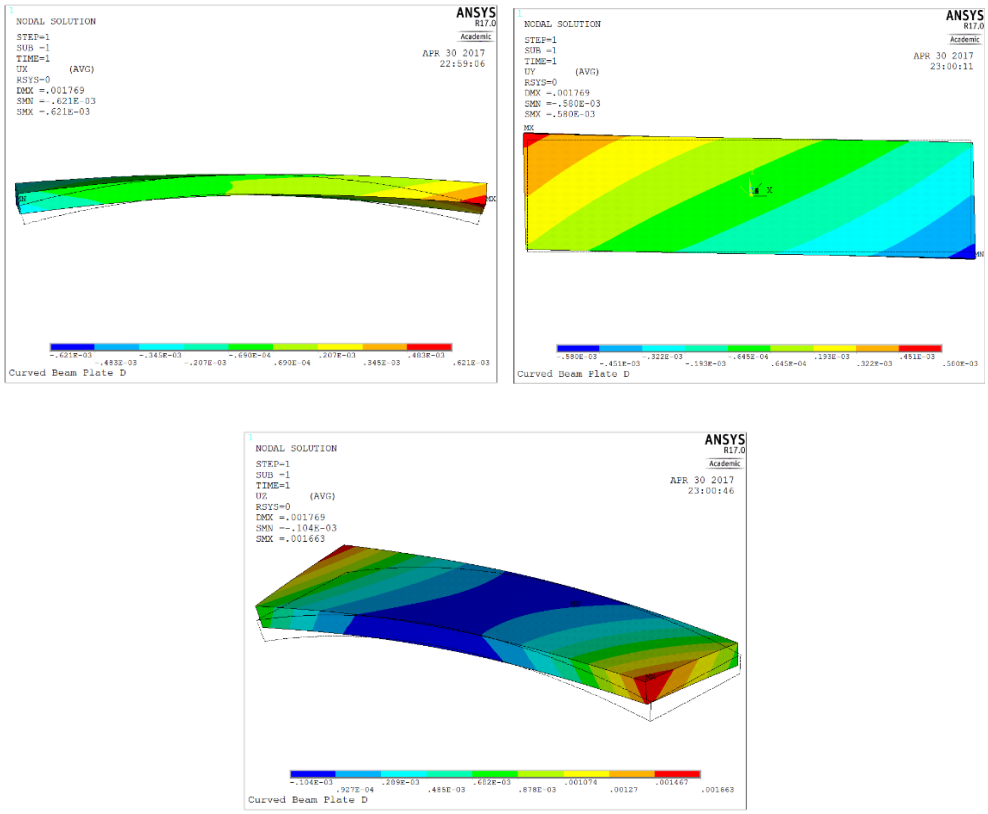

Figure 4.14 X, Y and Z Component Deformation for Curved Beam D

4.2.6 Change in Length/Radius

4.2.6.1 Nodes and Lines along X Direction

For obtaining the change in the length or radius of the curved beam, the lines are selected and the change in length is calculated from X component displacement the nodes connecting the lines. The lines, which are taken for analysis and the nodal points connecting them, are listed in the Table and Figure as below.

Table 4.16 Lines and Nodes used for Calculating Change in Length

Line	Node 1	Node 2
1	100	15200
2	119384	118941
3	119236	118942
4	101	7759

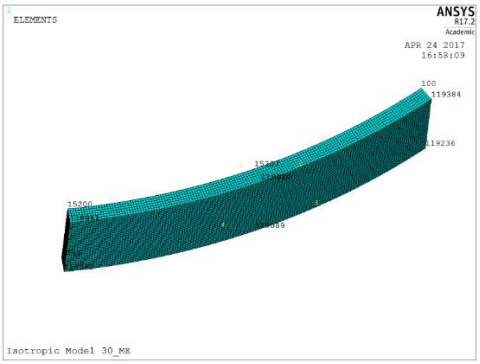

Figure 4.15 Lines used for Calculation of Change in Length / Radius

4.2.6.2 Results

The change in length (in inches) for the selected lines are given in Table 4.17 below.

Table 4.17 Change in Length of the Curved Beam (in inches)

Models / Lines	A	B	C	D
1	0.0439E-4	1.6574E-4	2.2624E-4	9.4552E-4
2	0.2371E-4	1.7408E-4	0.6119E-4	4.5621E-4
3	0.2371E-4	1.7408E-4	0.6119E-4	4.5621E-4
4	0.0439E-4	1.6574E-4	2.2624E-4	9.4552E-4

4.2.7 Change in Width of the Beam

4.2.7.1 Nodes and Lines along Y Direction

For obtaining the change in the width of the curved beam, the lines are selected and the change in length is calculated from Y component displacement the nodes connecting the lines. The lines, which are taken for analysis and the nodal points connecting them, are listed in the Table and Figure as below.

Table 4.18 Lines and Nodes used for Calculating Change in Width

Line	Node 1	Node 2
1	100	101
2	15307	7833
3	15200	7759
4	118941	118942
5	119310	119089
6	119384	119236

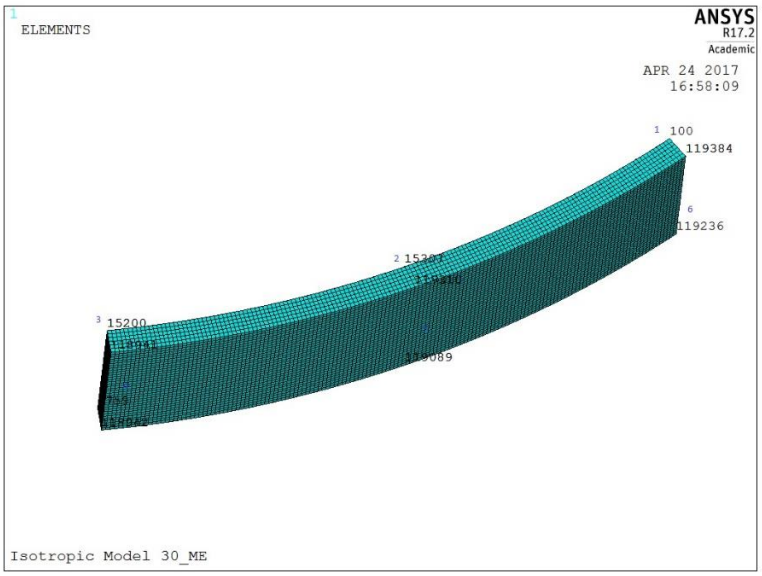

Figure 4.16 Lines 1-6 used for Calculation of Change in Width

4.2.6.2 Results

The change in width (in inches) for the selected lines are given in Table 4.19 below.

Table 4.19 Change in width of the Curved Beam (in inches)

Models / Lines	A	B	C	D
1	1.6264E-4	2.5575E-4	0.9887E-4	2.2431E-4
2	1.1082E-4	2.84E-4	0.7055E-4	2.585E-4
3	1.6264E-4	2.5575E-4	0.9887E-4	2.2431E-4
4	1.4429E-4	2.5924E-4	2.5872E-4	3.2172E-4
5	1.0811E-4	2.8132E-4	2.2544E-4	3.261E-4
6	1.4429E-4	2.5924E-4	2.5872E-4	3.2172E-4

4.2.8 Change in Thickness of the Beam

4.2.8.1 Nodes and Lines along Z Direction

For obtaining the change in the thickness of the curved beam, the lines are selected and the change in length is calculated from Z component displacement the nodes connecting the lines. The lines which are taken for analysis and the nodal points connecting them are listed in the Table and Figure as below.

Table 4.20 Lines and Nodes used for Calculating Change in Thickness

Line	Node 1	Node 2
1	100	119384
2	15307	119310
3	15200	118941
4	7759	118942
5	7833	119089
6	101	119236

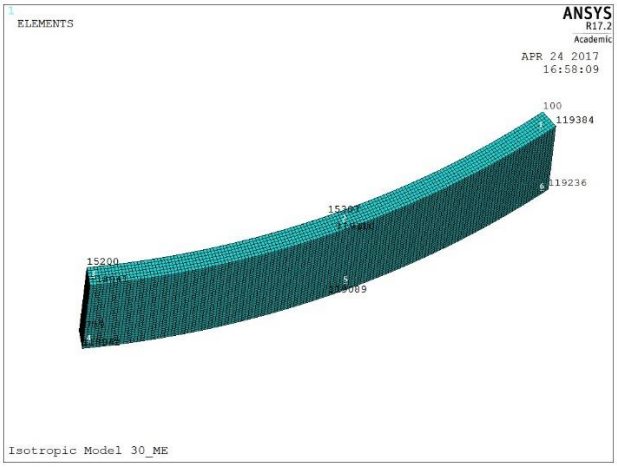

Figure 4.17 Lines 1-6 used for Calculation of Change in Thickness

4.2.8.2 Results

The change in thickness (in inches) for the selected lines are given in Table 4.21 below.

Table 4.21 Change in thickness of the Curved Beam (in inches)

Models / Lines	A	B	C	D
1	1.0332E-4	0.7811E-4	0.7953E-4	1.2154E-4
2	0.9493E-4	0.8523E-4	0.7724E-4	0.7725E-4
3	0.4708E-4	0.5981E-4	0.973E-4	1.494E-4
4	1.0332E-4	0.7811E-4	0.7953E-4	1.2154E-4
5	0.9493E-4	0.8523E-4	0.7724E-4	0.7725E-4
6	0.4708E-4	0.5981E-4	0.973E-4	1.494E-4

4.3 Parametric Study on Curved Beams

For better understanding on the Z-direction deformation and the thickness change of the curved beams, parametric analysis was carried out on the 3D FEM model. Different cases were considered, and the change in the deformation and thickness for every case was analyzed.

Rules are followed for parametric study :-

1. Since the model geometry is changed for each case, the mesh should be maintained in the ratio of 2 : 1 : 1 for the length, breadth and thickness of each element.
2. The mesh convergence criteria was carried out to verify that the model is fully constrained.
3. The model was validated again with the isotropic material properties.

4.3.1 Varying Radius of Curvature for Different Temperature Loads.

Assuming the same boundary conditions which was used for our preliminary analysis, the inner radius of the curved beams is varied by r = 2, 3 and 4 inches. The temperature load is applied as a steady state increase, in the range of ΔT = 50°F, 100°F and 150°F, respectively.

4.3.1.1 Change in Thickness

The change in the thickness for each case is calculated for the lines along the thickness direction, as shown in Figure 4.17 and Table 4.20

In observation, the change in the thickness values of line 4, 5 and 6 are same as 1, 2 and 3 respectively. This indicates that the values are symmetric about the diagonal axis. Hence, for simpler observation, the change in thickness of line 1, 2 and 3 are calculated and is depicted as follows.

Line 1 – Upper Right Corner of the Curved Beam

Line 2 – Upper Middle Line of the Curved Beam

Line 3 – Upper Left Corner of the Curved Beam

Line 4 – Lower Left Corner of the Curved Beam

Line 5 – Lower Middle Line of the Curved Beam

Line 6 – Lower Right Corner of the Curved Beam

Results from Line 1 = Line 4

Line 2 = Line 5

Line 3 = Line 6

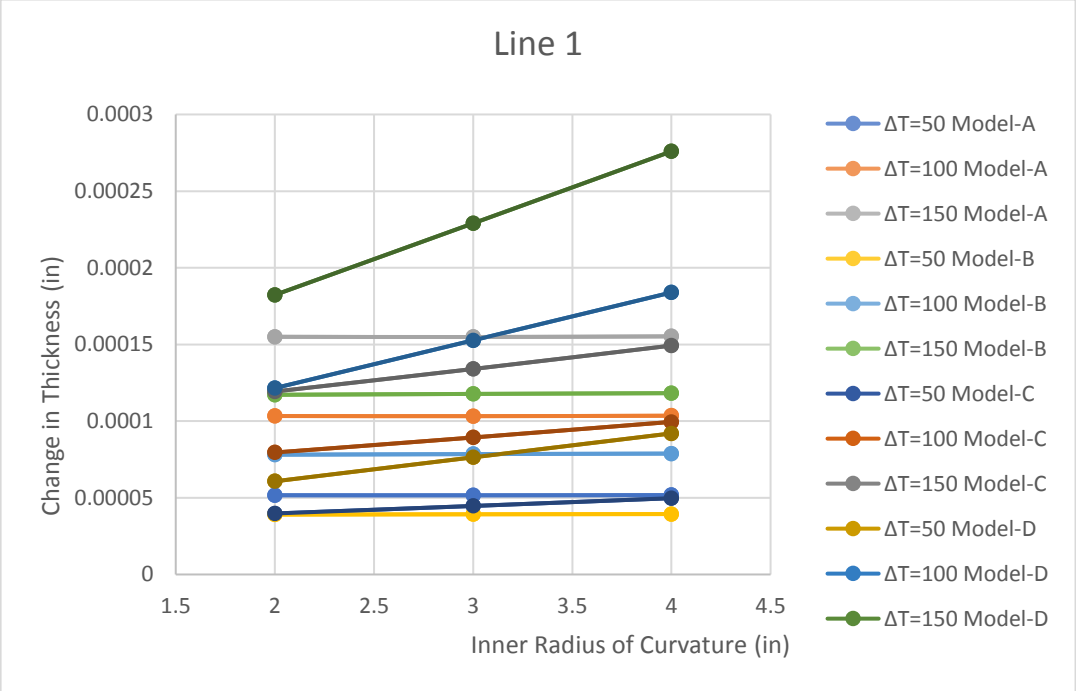

Figure 4.18 Change in Thickness of Line 1 for Case 1

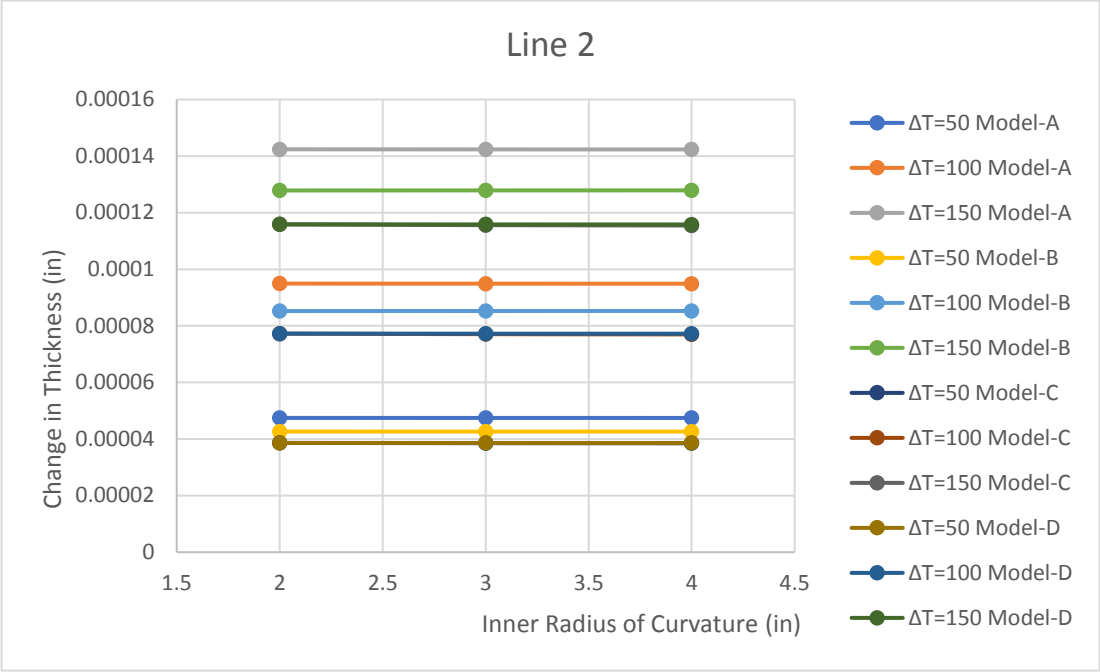

Figure 4.19 Change in Thickness of Line 2 for Case 1

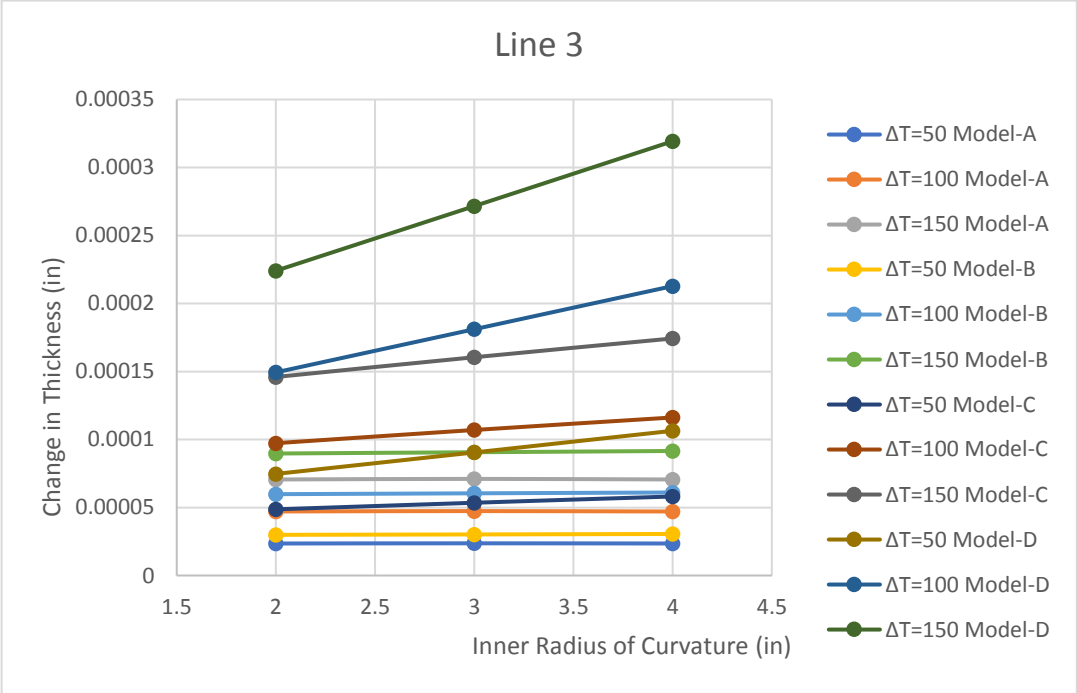

Figure 4.20 Change in Thickness of Line 3 for Case 1

From Figures 4.26, 4.27 and 4.28, we can observe that the change in thickness of the curved beam at the middle does not change for increase in radius. Observing line 1 and 2, the thickness change is negligible for models A and B which are symmetrical laminates. There is quite change in thickness observed for model C – un-balanced symmetrical laminate and huge thickness difference for model D – un-balanced un-symmetrical laminate. The effect of temperature difference gives us a linear relationship. The observation is same for all the three temperature ranges.

4.3.1.2 Z – Component Deformation

The Z component deformation of the inner area of the curved beam is observed for all the cases mentioned above. Four nodal points at the four corners of the inner radius is selected.

Table 4.22 Location of the Nodes for Case 1

Node	X (in)	Y (in)	Z (in)	Location
100	0.51764	0.12500	-0.89478E-1	Right Back (RB)
101	0.51764	-0.12500	-0.89478E-1	Right Front (RF)
7759	-0.51764	-0.12500	-0.89478E-1	Left Front (LF)
15200	-0.51764	0.12500	-0.89478E-1	Left Back (LB)

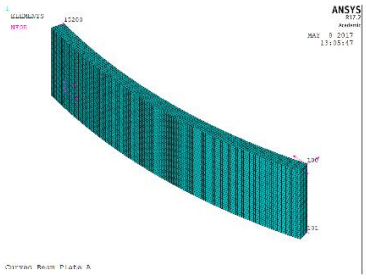

Figure 4.21 Nodes for Z-Component Deformation for Case 1

Again, In observation, the deformation at nodes 100 and 101 are identical with nodes 7759 and 15200, respectively, proving the symmetrical nature about the diagonal of the curved beam.

Node 100 = Node 7759

Node 101 = Node 15200

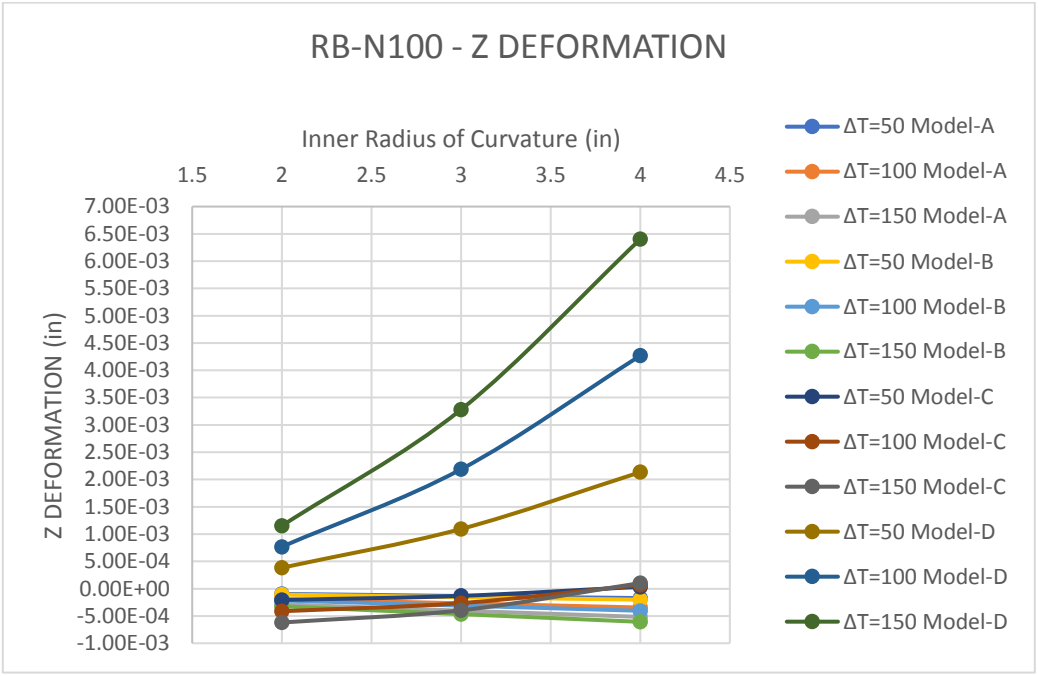

Figure 4.22 Z component Deformation at node 100,7759 for case 1

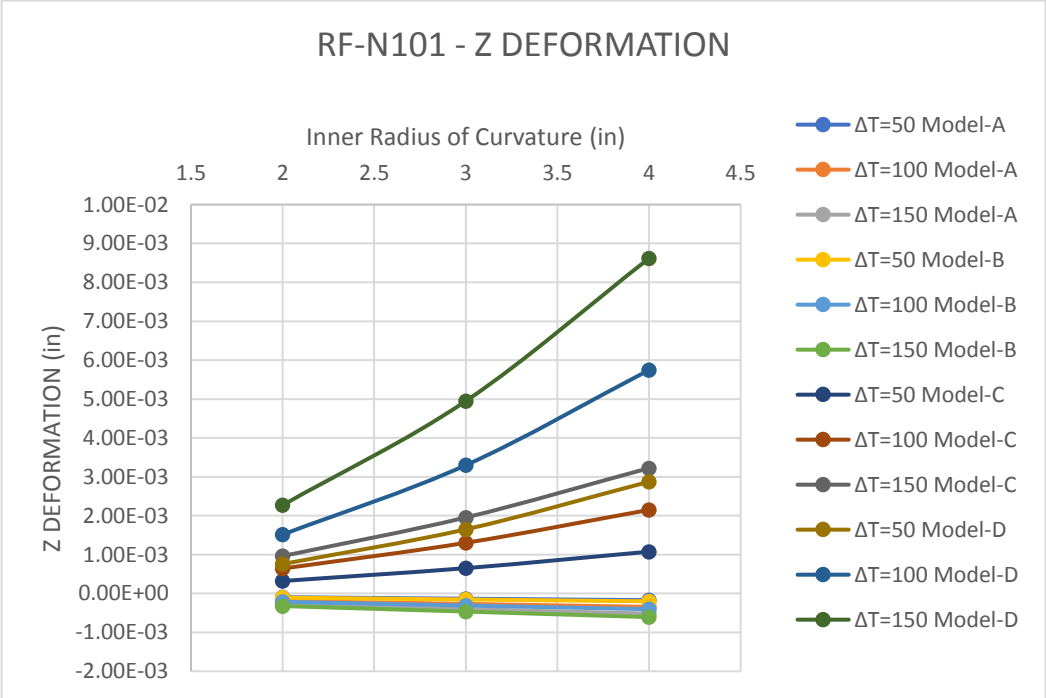

Figure 4.23 Z Component deformation at node 101, 15200 for case 1

Although the values differ for the Figures 4. And 4. , the pattern of the deformation of the nodes of the inner area are same. The curved beams A and B has the negative component of deformation on both nodes, indicating that the inner radius decreases. The curved beam C – un-symmetrical balanced laminate has both negative and positive components of deformation in Z direction. The change in the deformations for increase in the radius of curvature is also observed. For curved beam D – un-symmetrical un-balanced laminate, the deformation towards the positive Z direction and the change in deformation increases rapidly with increase in radius.

4.3.2 Varying Width of the Curved Beam for Different Temperature Loads

This case study involves the analysis of curved beam, by varying the width of the curved beam. By varying the width, the width to thickness ratio is also varied, hence the curved beam is changed from the narrow beam to wide beam for width = 0.4 inch. The thickness of curved beam is 0.0432 inch.

Table 4.23 Varying Widths and W/T Ratio for Case 2

Width (in)	Width/Thickness
0.1	2.32
0.2	4.63
0.25	5.78
0.3	6.95

4.3.2.1 Change in Thickness of Curved Beam due to w/t ratio

The lines that were used for this parametric study are shown in Figure 4.24. The results obtained from line 1 and 2 are equal to the results from line 4 and 5 indicating that they are symmetrical about the diagonal axes. Line 3 is the line at the center of the curved beam.

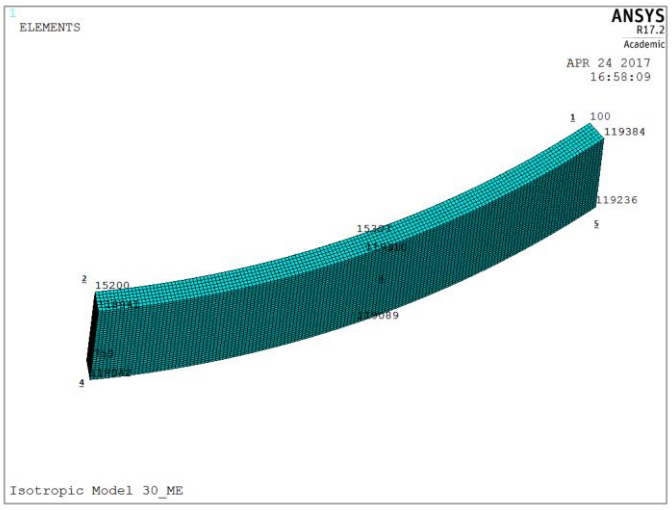

Figure 4.24 Lines for observing Change in Thickness for Case 2

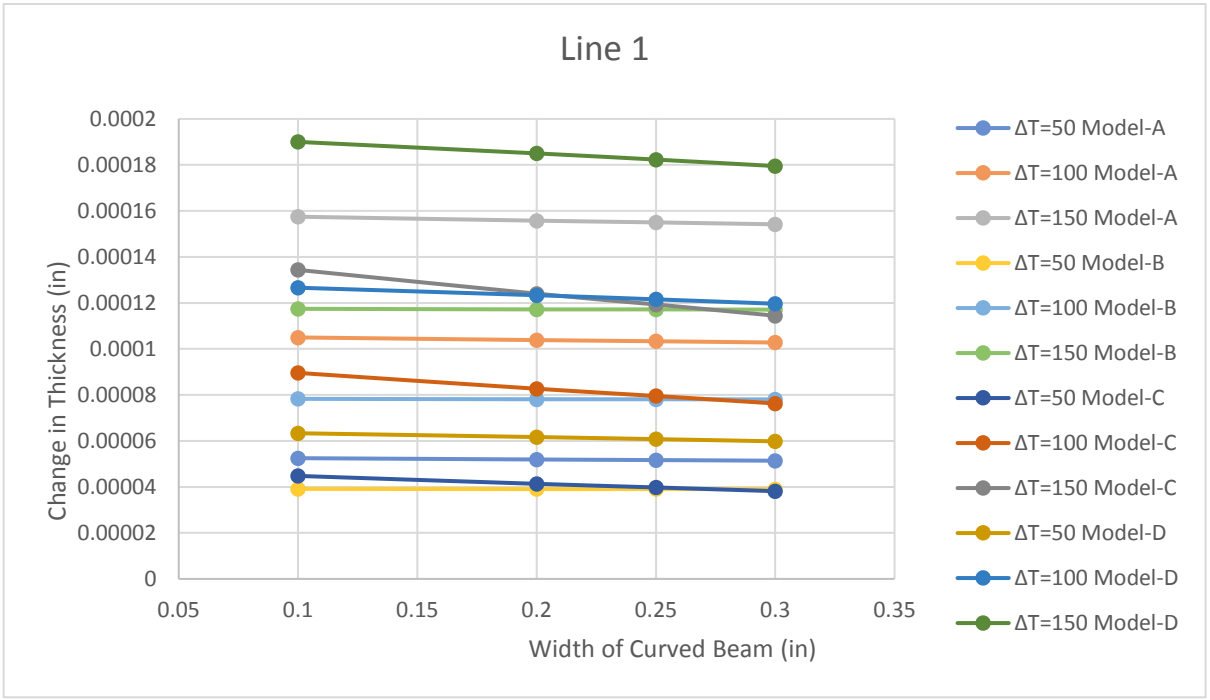

Figure 4.25 Change in Thickness of Line 1 and 4 for Case 2

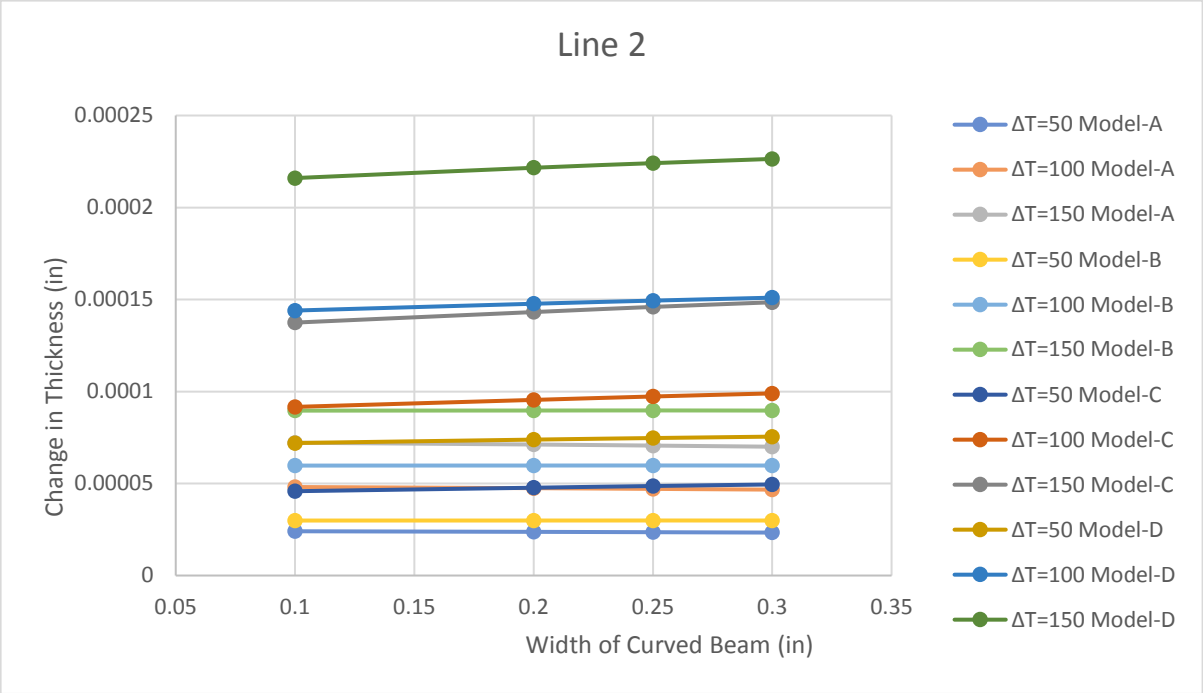

Figure 4.26 Change in Thickness of Line 2 and 5 for Case 2

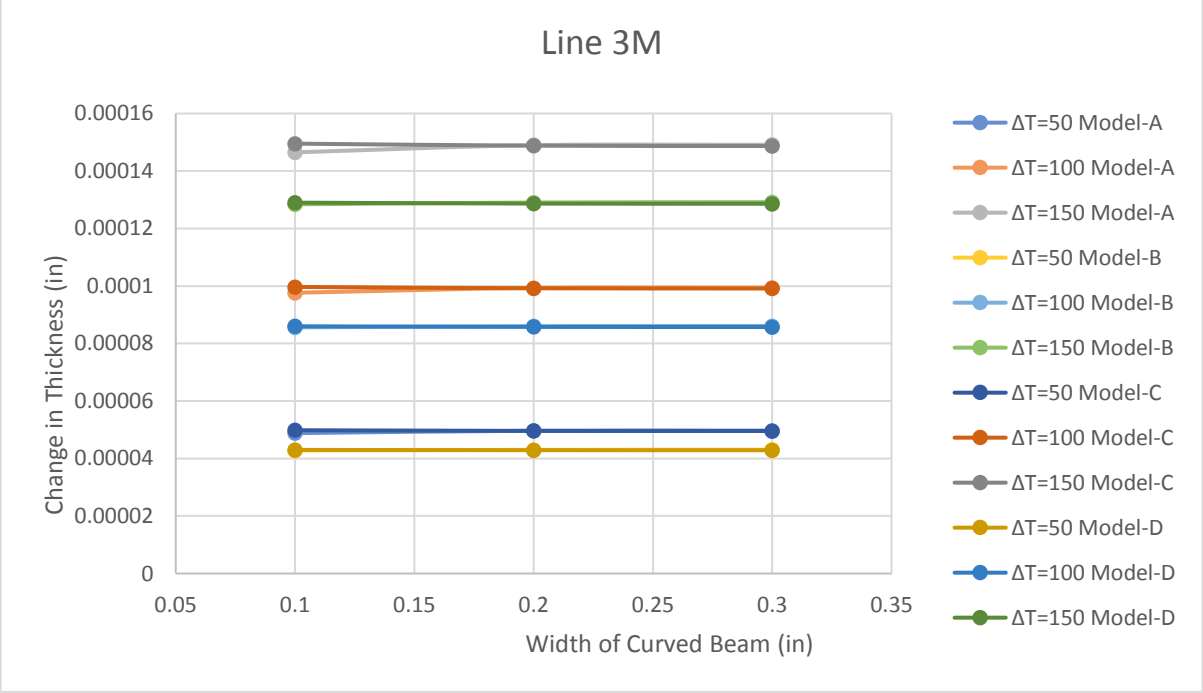

Figure 4.27 Change in Thickness of line 3 for Case 2

Similar to the previous case, the change in thickness with varying width of the curved beam for Model A and Model B are negligible. Also the there is no increase of change in thickness at the center of the curved beam. The change in thickness for Models C and D are a linear relationship, it increases or decreases based on the location of the line.

4.3.2.2 Z- Component Deformation of Nodes

As discussed in Case 1, the deformation at nodes 100 and 101 are identical with nodes 7759 and 15200 respectively, proving the Symmetrical nature about the diagonal of the curved beam.

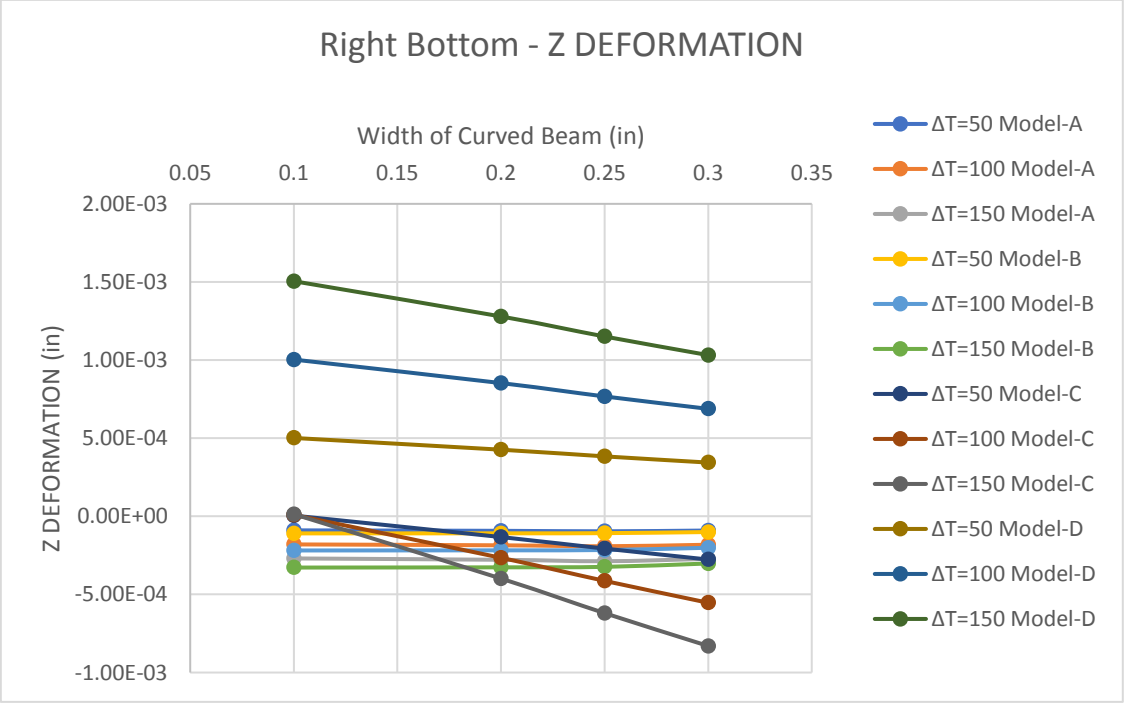

Figure 4.28 Z component Deformation of Node 100 and 7759 for Case 2

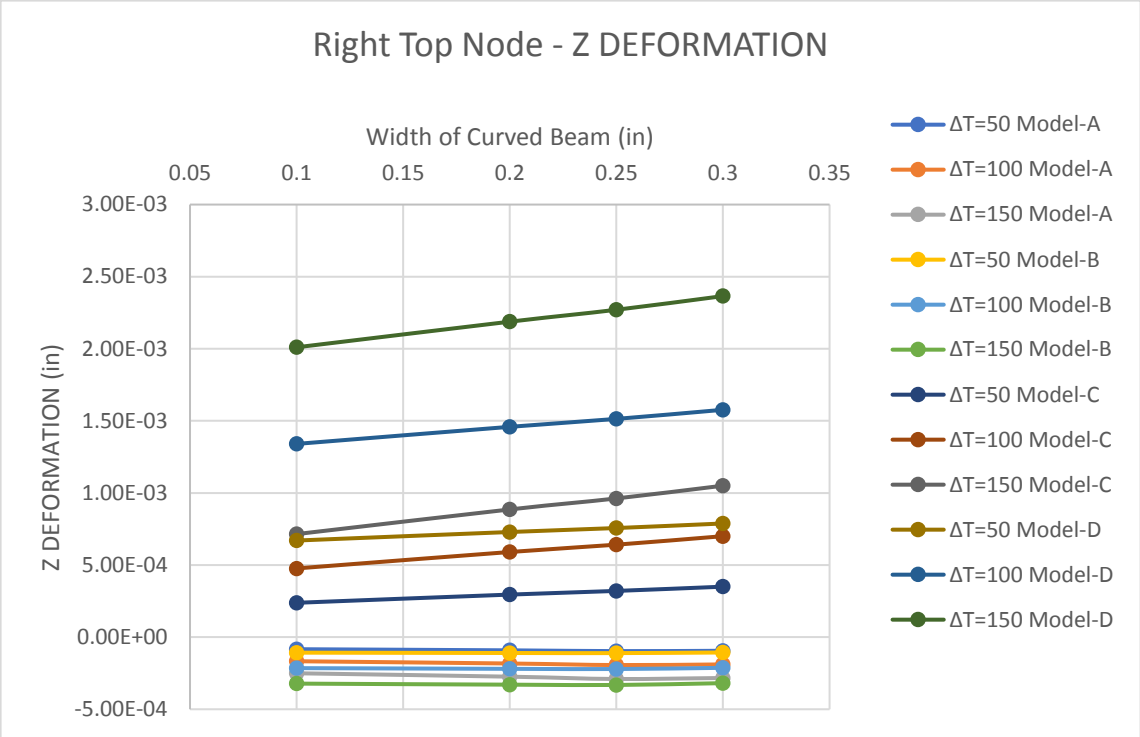

Figure 4.29 Z Component Deformation of Node 101 and 15200 for Case 2

The Z Component deformation of the curved beam for Models C and D decrease at node 100,7759, increases at node 101,15200 for the change in the width of the curved beam. The symmetrical pattern of the deformation along the diagonal of the curved beam is well observed for all values of temperature.

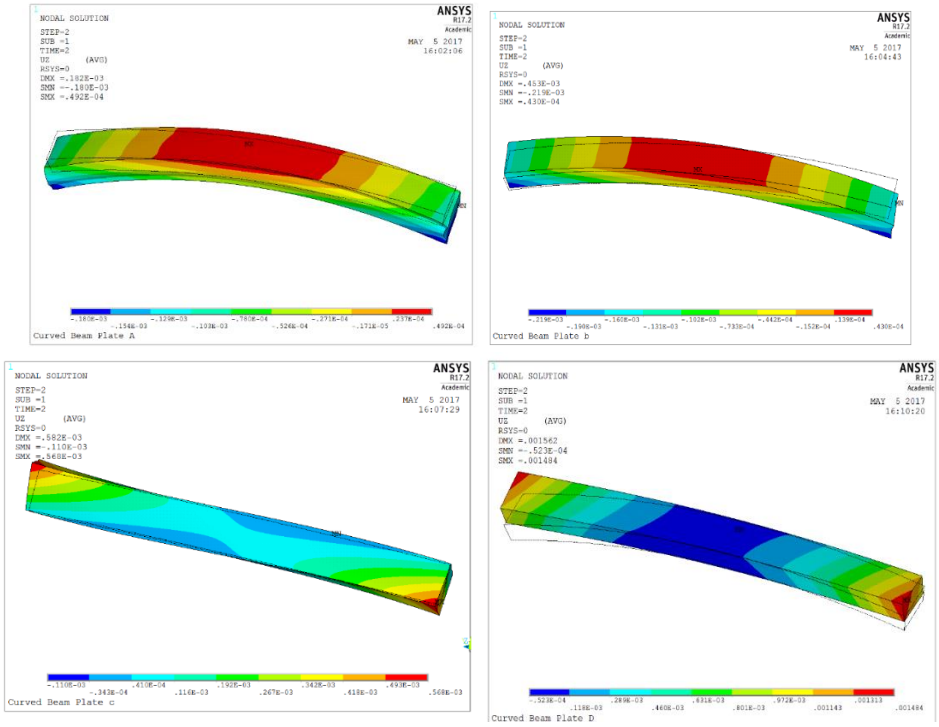

Figure 4.30 Curved Beam with Width of 0.1 inch for Case 2

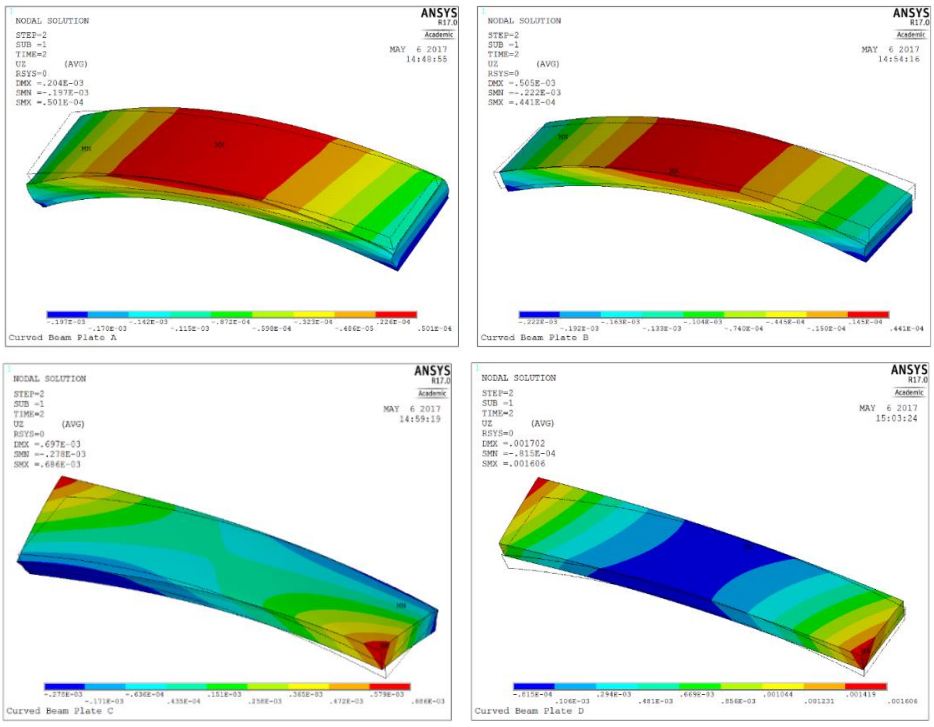

Figure 4.31 Curved Beam with Width 0.2 inch for Case 2

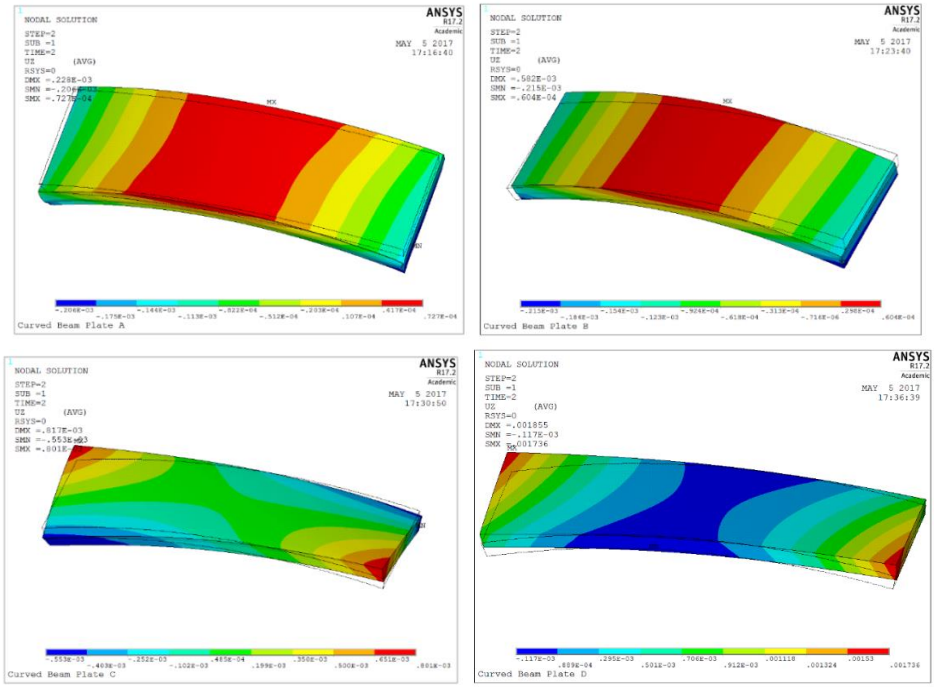

Figure 4.32 Curved Beam with Width 0.3 inch for Case 2

4.3.3 Fixed on Both Edges Parallel to Y-Z Plane

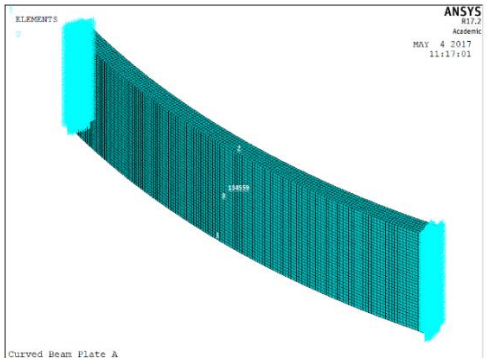

Figure 4.33 Boundary Conditions, Lines and Node for Case 3

In this study, the curved beam is constrained completely on the edges that are parallel to the Y-Z plane. The change in thickness is calculated in lines 1,2 and 3 which are the lines on the front, back and middle edge surfaces parallel to the X-Y plane. It was observed that the results from lines 1 and 2 are the same. The Z-component deformation was obtained at Node 134559, which is the center node on the top surface of the curved beam.

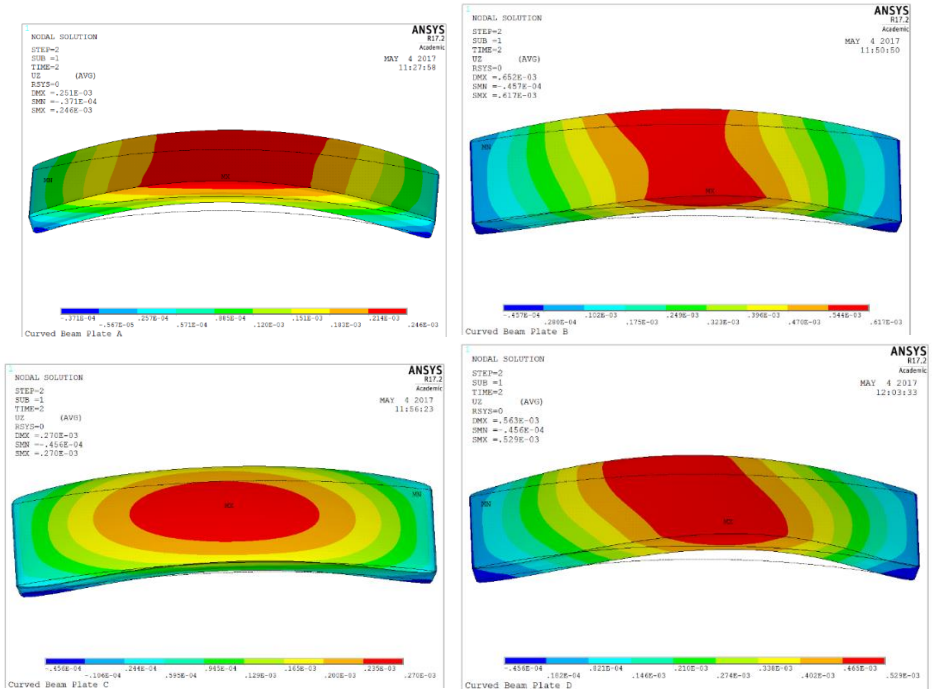

Figure 4.34 Z-Component Deformation of Curved Beams for Case 3

4.3.3.1 Change in Thickness for Case 3

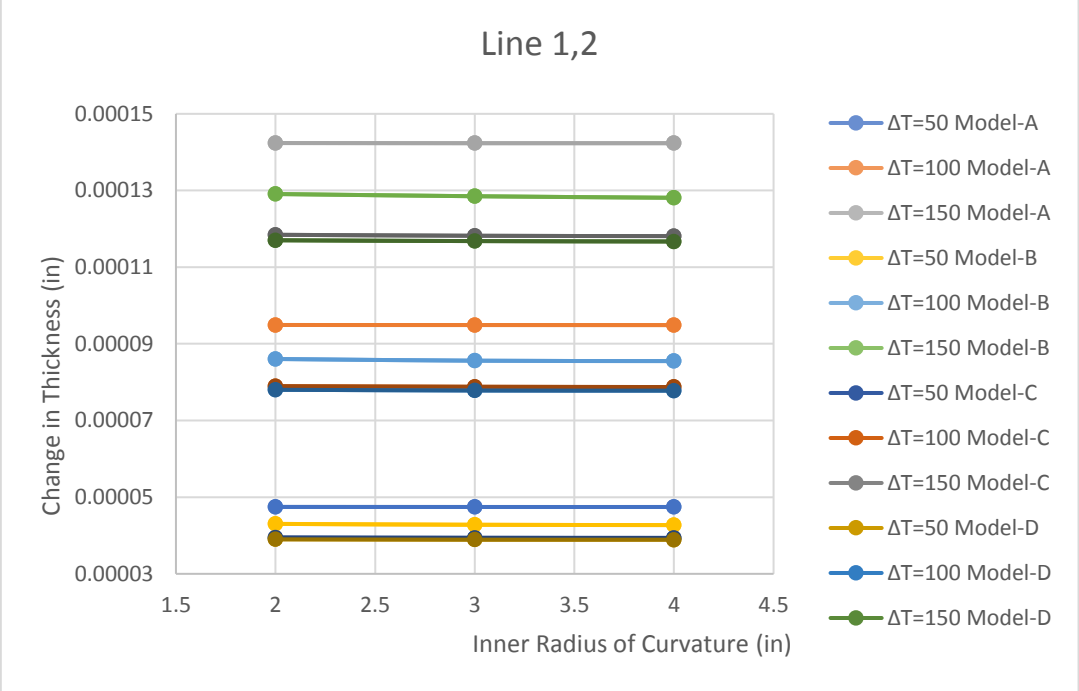

Figure 4.35 Change in Thickness of Line 1 and 2 for Case 3

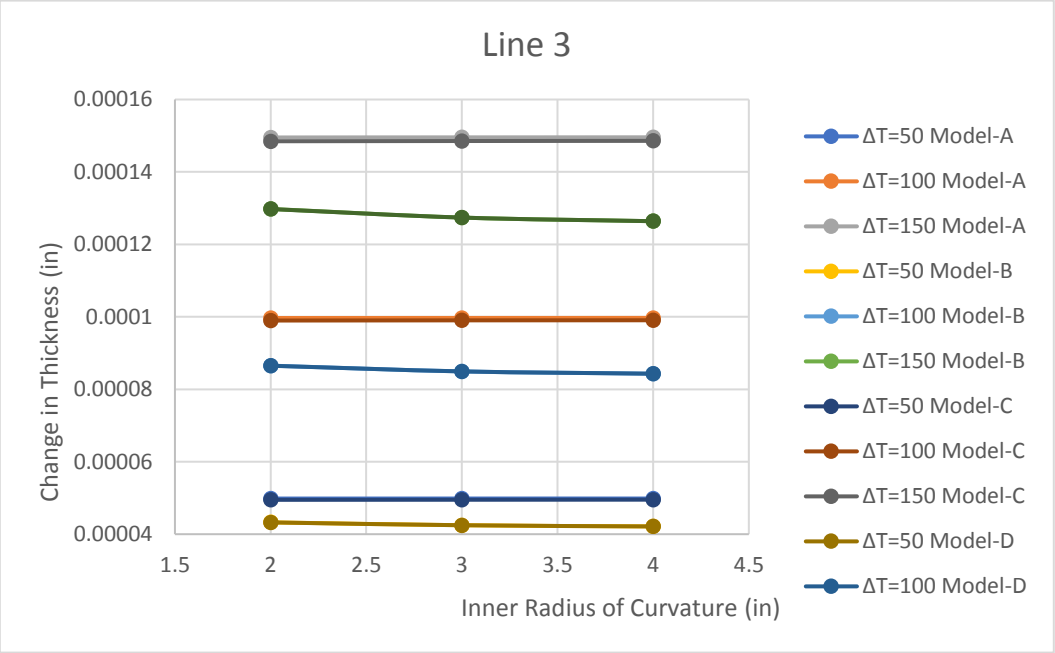

Figure 4.36 Change in Thickness of line 3 for Case 3

4.3.3.2 Z-Component Deformation for Case 3

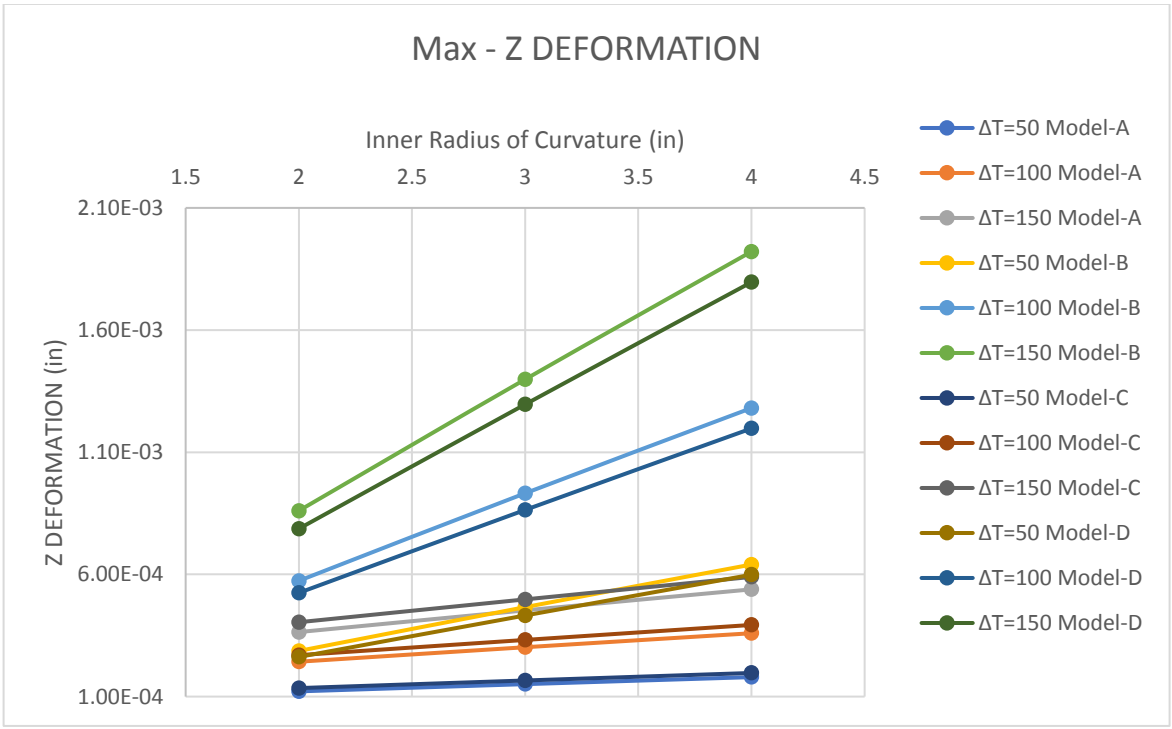

Figure 4.37 Z Deformation at Mid-center Node of Upper Surface for Case 3

There is not much change in difference of the thickness with increase in radius of the curved beam, when the curved beam is constrained in the edges parallel to the Y-Z Plane. The maximum deformation of the curved beam as observed at the mid-center of the upper surface, increases with the increase in the inner radius of curvature. The increase is observed to be large for the un-balanced laminates B and D than the balanced laminates A and C.

4.3.4 Fixed on Both Edges Parallel to X-Z Plane

In this study, the curved beam is constrained completely on the edges that are parallel to the X-Z plane. The change in thickness is calculated in lines 1,2 and 3 which are the lines on the front, back and middle edge surfaces parallel to the X-Z plane. It was observed that the results from lines 1 and 2 are the same. The Z-Component deformation was obtained at Node 134559, which is the center node on the top surface of the curved beam

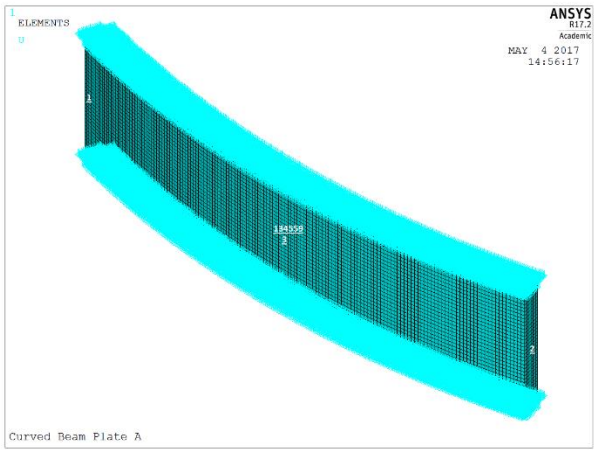

Figure 4.38 Boundary Conditions, Lines and Node for Case 4

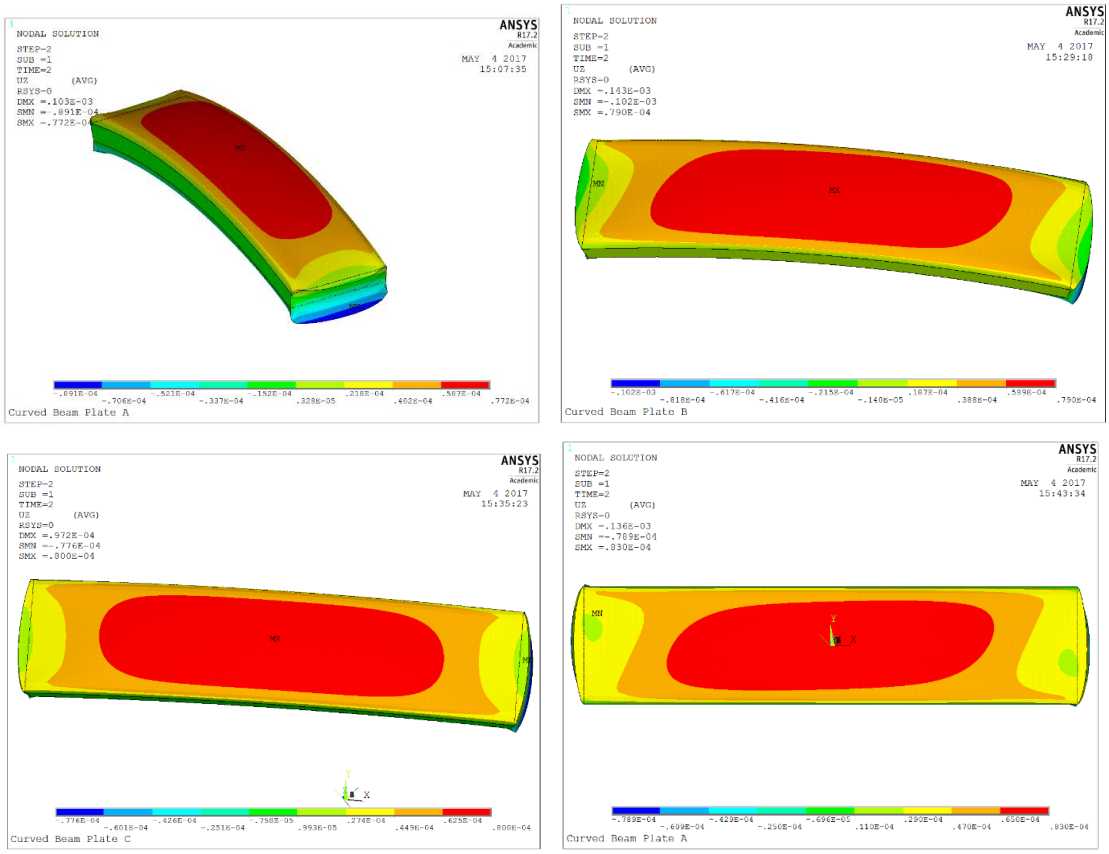

Figure 4.39 Z-Component Deformation of Curved Beams for Case 4

4.3.4.1 Change in thickness for Case 4

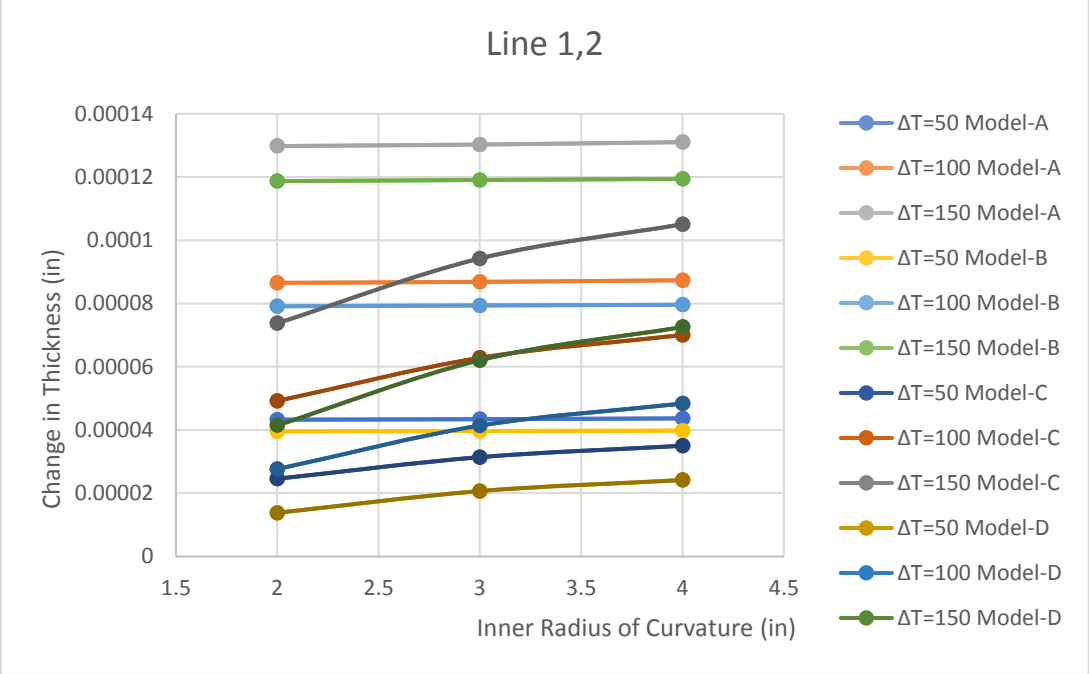

Figure 4.40 Change in Thickness of Line 1 and 2 for Case 4

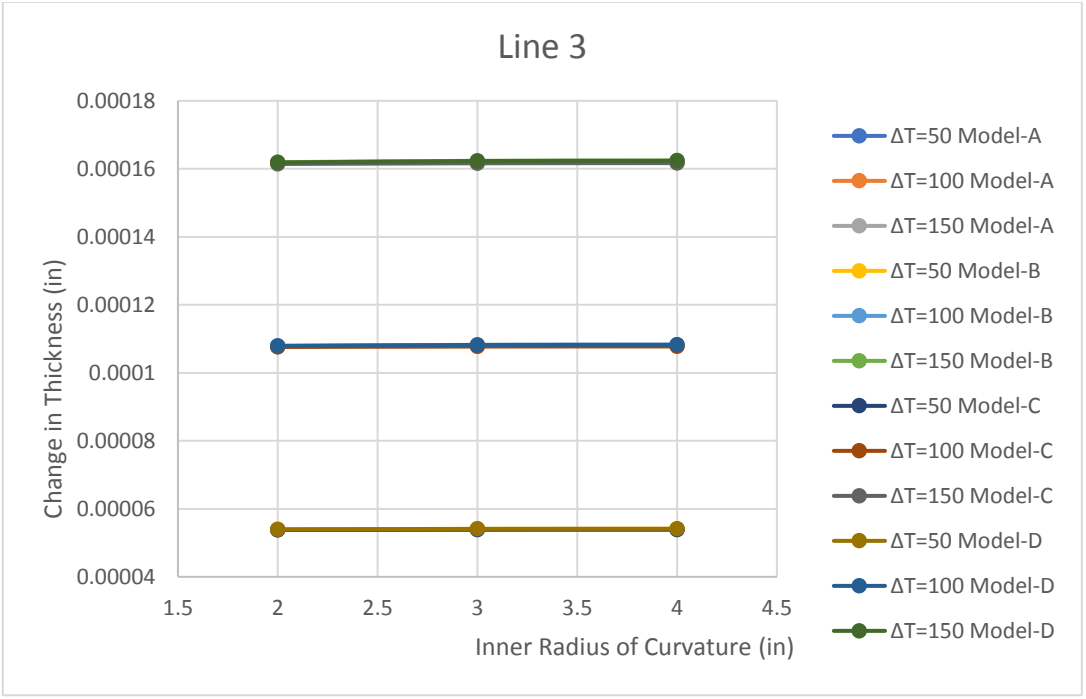

Figure 4.41 Change in Thickness of Line 3 for Case 4

4.3.4.2 Z-Component Deformation for Case 4

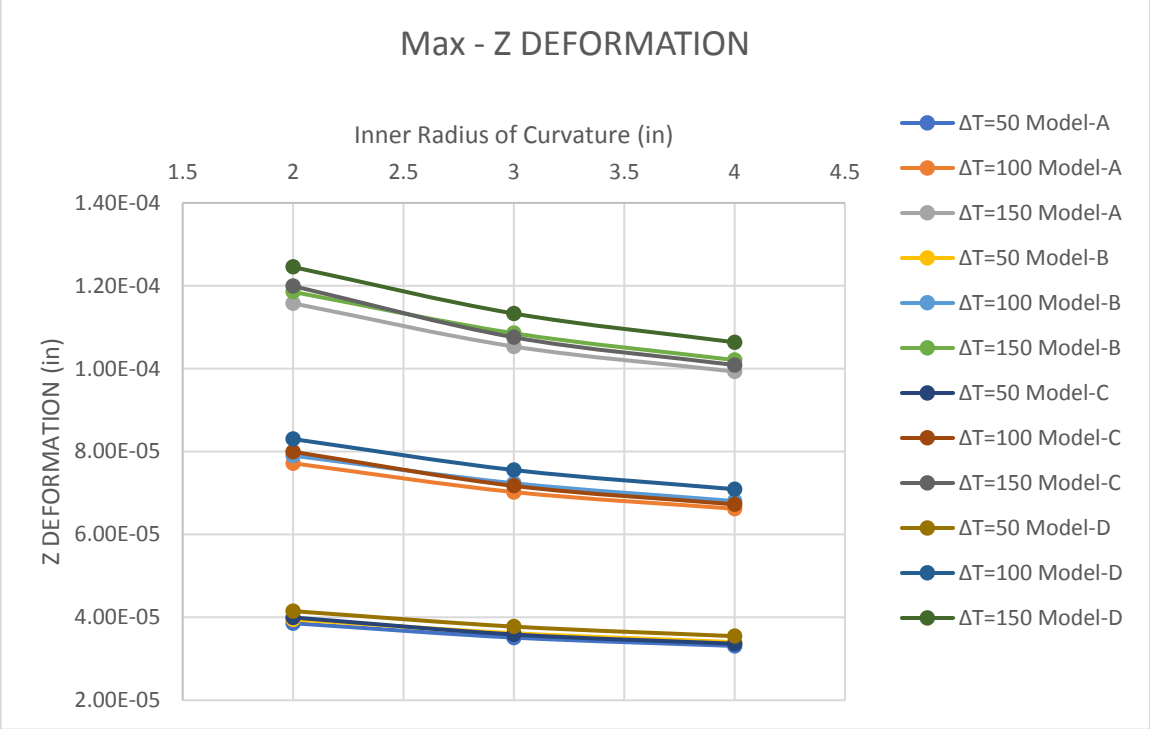

Figure 4.42 Z-Component Deformation at Mid-Center Node of Upper Surface for Case 4

When the curved beam is constrained in the edges parallel to the X-Z plane, there is no increase of change in thickness for increase in radius for the models A and B. For model C and D, there is a curvilinear increase of change in thickness with the increase in radius. The Z – component of the deformation as observed at the mid-center node 134559, decreases for all the models with increase in radius, which is inverse to the previous case.

Chapter 5

CONCLUSION AND FUTURE WORK

This research work focuses on the deformation effects in the composite structures due to the thermal environments. Flat laminates and curved beams are the composite structures that are considered for the analysis. The analytical solution for determining the deformation and stresses of the laminates and curved beams under temperature environment are derived by using the modified Classical Lamination Plate Theory. The constitutive equation for the curved beam element was converted to the global constitutive equation for curved beam by the parallel axes theorem and integrating over the circumference of the element. The stresses, mid-plane strain and curvature values were obtained and the displacement was calculated. Since the laminated plate/curved beam used in this study are thin, the plane stress condition are assumed. Because of this, only 2-D in-plane properties were used to determine the in-plane deformation. For determining the deformation in thickness direction, the 3rd dimensional properties were used. 2D and 3D finite element modelling was done in Ansys 17.0 and 17.2 versions. 2D shell model was created which was a smeared model. 3D model was created as a layer by layer model, to obtain more accurate results on the deformation of each individual ply and the structure. Mesh convergence analysis was carried out and the finite element model was validated using the isotropic material properties.

After validating the results from the analytical and finite element models, parametric studies was carried out on the curved beams with increasing the radius of curvature, change in the temperature environments, and change in the width to thickness ratio of the curved beams and by applying fixed constraints on the edges of the curved beam.

The conclusions that are observed in this thesis are

- The Z component of deformation for symmetrical laminates is uniform throughout the region of the laminate and the curved beam except near its edge, since the 3rd dimensional stresses exist at the edge.
- The Z component of deformation for unsymmetrical laminates is not uniform throughout the region of the laminate and curved beam, due to bending and curvature effects.
- The X, Y and Z component of deformation are equal at equi-distant point of a line which passes through the center of the composite structure.
- The 3D layer by layer finite element model gives more accurate results of deformation and ply stresses than that of the 2D smeared shell finite element model.
- The change in the thickness of the curved beam is constant with increase in the radius of the curvature or increase in width to thickness ratio for the symmetrical layup, and increases or decreases for the un-symmetrical layup of plies.
- The Z component of deformation increases with increase in radius of curvature, when the curved beam edges parallel to Y-Z plane are constrained and decreases with increase in radius of curvature, when the curved beam edges parallel to X-Z plane are constrained.

Future work can be done on the double curvature curved beam models, obtaining analytical expressions using the classical lamination shell theory and the beam theory, changing the stacking sequences. Experimental verification of the results is also recommended. Thermal analysis including time dependent properties can also be done.

References

1. Hyer, M W., Vogl, G A., “Response of elliptical composite cylinders to a spatially uniform temperature change”, Elsevier Composite Structures 51 (2000) 169-179
2. Dano, M L., Hyer, M W., “Thermally Induced Deformation Behavior of Unsymmetric Laminates”, Int. J. Solids Structures Vol 35 No 17, pp 2101-2120, 1998
3. Hyer, M W., “Stress Analysis of Fiber Reinforced Composite Materials”
4. Duan, B**.,** Motagaly, K A., Guo, X., Mei C., “Flutter and Thermal Deflection Suppression of Composite Plates Using Shape Memory Allow”, AIAA Journal Vol.43 No 9 September 2005
5. Khdeir, A A., Rajab, M D., Reddy, J N., “Thermal effects on the response of cross ply laminated shallow shells” Int. J. Solid Structures – Vol 29. No.5 pp 653-667,1992
6. Patel, B P., Shukla, K K., Nath, Y., “Thermal Post buckling Analysis of Laminated cross ply truncated circular conical shells”, Elsevier Composite Structures 71 (2005) 101-114
7. Chitikela, N S L., Eslami H., Radosta, F., “An Analytical Investigation of Natural Frequency for a Symmetric Composite Box-Beam with Thermal Effects”, 52nd AIAA/ASME Structures and Materials 2011
8. Chang, X., Lie, J., Ren J., “Thermal Post buckling of heated cross ply laminated composite beams”, Applied Mechanics and Materials Vol 105-107 (2012) pp 2321-2324.
9. Xiang, S., Chen Y T., “Thermal Bending of Laminated Composite Plates by a meshless method”, Applied Mechanics and Materials Vol 433-435 (2013) pp 2008-2011

10. Mackerle, J., “Finite Element Analyses of sandwich structures-a bibliography (1980-2001)” Engineering Computations 2002;19,1/2.
11. Li, X., Zhao, Y., (2010), “Three Dimensional Exact solutions for In-Plane Curved Beams with Pinned-Pinned Ends under Thermal Load”, Twentieth International Offshore and Polar Engineering Conference.
12. Roos, R., Hormann, M., and Behrens, C S., “Shell and Solid Modelling of Composite Structures as a Base for Simulation driven Optimization Processes”, June 2011, CADFEM GmbH CFK Valley Stade Convention
13. Agarwal, M., (2016) “Analysis of Curved Composite Beam”, Master Thesis, West Virgina University.
14. Chan, W., and Demirhan, C., “A Simple Closed-Form Solution of Bending Stiffness for Laminated Composite Tubes,” Journal of Reinforced Plastics and Composites, Vol. 4, March 1, 2000.
15. Chia Wei Su and Chan, W., (2007) “Thermal Stresses of Composite Beams with Rectangular and tubular cross sections”
16. Nyugen, T., and Chan, W., (2010) “Effects of curvature on the stresses of a curved laminated beams subjected to bending”, Master Thesis, University of Texas at Arlington
17. Mahadev, S., and Chan, W., “ Closed-Form Analytical Method for Analyzing Laminated Composite Tubes in Hygrothermal Environment, 54th AIAA/ASME/ASCE/AHS/ASC Structures, Structural Dynamics and Materials Conference, 8th -11th April 2013, Boston, Massachusetts, USA.
18. Lu, W T., and Chan, W., (2015), “Effects of transverse shear deformation on maximum deflection of composite beams with various laminate configurations and boundary conditions”, Master Thesis, The University of Texas at Arlington

19. Daniel, I.M. and Ishai, O., Engineering Mechanics of Composite Materials, 2nd edition, Oxford University Press, 2006.
20. Chan W. S., Composite Lecture Notes, University of Texas at Arlington, Fall 2015 and Spring 2016.
21. J. R. Vinson, R. L. Sierakowski, ”Composite Material Shells”, Mechanics of Structural Systems pp 149-172.
22. ANSYS Documentation – www.ansys.com – Element Reference Manual
23. Alamgir, F., and Chan W S., “Issues on finite element modeling of laminated composite structures”, Master Thesis, The University of Texas at Arlington.
24. Su, C W., and Chan W S., “Thermal stresses of composite beams with rectangular and tubular cross-sections”, Master Thesis, The University of Texas at Arlington
25. Flugge, W., (1966), “Stresses in Shells” New York - Splinger-Verlag Inc.

Biographical Information

Muthu Ram Prabhu Elenchezhian, born on 18th December of 1993, completed his Bachelor of Engineering in Aeronautical Engineering from Hindusthan College of Engineering and Technology, affiliated to Anna University, Chennai, India on May 2015.

He pursued his Masters in Aerospace Engineering at The University of Texas at Arlington starting August 2015. He worked on his master's thesis research work under the supervision of Dr. Wen S Chan starting August 2016.His research interest includes composite structures, finite element modelling, manufacturing of composites, damage tolerance and predictability of composite materials. During his master's degree at UTA, he worked as Research Intern in the Institute for Predictive Performance Methodologies at The University of Texas at Arlington Research Institute.

He graduated with his master's degree from UTA in August 2017. Starting August 2017, He plans to begin with his Doctoral Degree in Aerospace Engineering at UTA, under the supervision of Dr. Kenneth Reifsnider and Dr. Ashfaq Adnan.